Ligand binding determines proteolytic stability of *Vibrio* LuxR/HapR quorum sensing transcription factors

Running title: Quorum sensing inhibition in *Vibrio vulnificus*

Tanmaya A. Rasal[1], Caleb P. Mallery[2], Matthew W. Brockley[3], Laura C. Brown[5], Jon E. Paczkowski[2,3*], Julia C. van Kessel[1*]

1. Department of Biology, Indiana University, Bloomington, IN.
2. Department of Biomedical Sciences, University of Albany, Albany, NY.
3. Division of Genetics, Wadsworth Center, New York State Department of Health, Albany, NY.
4. Department of Chemistry, Indiana University, Bloomington, IN

* Corresponding authors:
Dr. Julia van Kessel
Biology Building 425K, Department of Biology, Indiana University
1001 E 3rd Street, Bloomington, IN 47405
Email: jcvk@indiana.edu
Telephone: 812-856-2235

Dr. Jon Paczkowski
David Axelrod Institute LSIB 5221, Division of Genetics, Wadsworth Center, NYSDOH
120 New Scotland Avenue, Albany, NY 12208
Email: jon.paczkowski@health.ny.gov
Telephone: 518-474-5484

Keywords: Quorum sensing, Quorum sensing inhibitors, Vibrio vulnificus, SmcR, HapR, LuxR, thiophenesulfonamides, protease

ABSTRACT

In *Vibrio* species, quorum sensing signaling culminates in the production of a TetR-type master transcription factor collectively called the LuxR/HapR family, which regulates genes required for colonization and infection of host organisms. These proteins possess a solvent accessible putative ligand binding pocket. However, a native ligand has not been identified, and the role of ligand binding in LuxR/HapR function in *Vibrionaceae* is unknown. To probe the role of the ligand binding pocket, we utilize the small molecule thiophenesulfonamide inhibitor PTSP (3-**p**henyl-1-(**t**hiophen-2-yl**s**ulfonyl)-1*H*-**p**yrazole) that we previously showed targets LuxR/HapR proteins. Amino acid conservation in the ligand binding pocket determines the specificity and efficacy of PTSP inhibition across *Vibrio* species. Here, we used structure-function analyses to identify PTSP-interacting residues in the ligand binding pocket of SmcR – the *Vibrio vulnificus* LuxR/HapR homolog – that are required for PTSP inhibition of SmcR activity *in vivo*. Forward genetic screening combined with X-ray crystallography structural determination of SmcR bound to PTSP identified substitutions at eight residues that were sufficient to reduce or eliminate PTSP-mediated SmcR inhibition. Small-angle X-ray scattering and computational modeling determined that PTSP drives allosteric unfolding at the N-terminal DNA binding domain. We discovered that SmcR is degraded by the ClpAP protease in the presence of PTSP *in vivo*; substitution of key PTSP-interacting residues stabilized or increased SmcR levels in the cell. This mechanism of inhibition is observed for all thiophenesulfonamide compounds tested and against other *Vibrio* species. We conclude that thiophenesulfonamides specifically bind in the ligand binding pocket of LuxR/HapR proteins, promoting protein degradation and thereby suppressing downstream gene expression, implicating ligand binding as a mediator of LuxR/HapR protein stability and function to govern virulence gene expression in *Vibrio* pathogens.

SIGNIFICANCE

LuxR/HapR proteins were discovered in the 1990s as central regulators of quorum sensing gene expression and later discovered to be conserved in all studied *Vibrio* species. LuxR/HapR homologs regulate a wide range of genes involved in pathogenesis, including but not limited to genes involved in biofilm production and toxin secretion. As archetypal members of the broad class of TetR-type transcription factors, each LuxR/HapR protein has a predicted ligand binding pocket. However, no ligand has been identified for LuxR/HapR proteins that control their function as regulators. Here, we used LuxR/HapR-specific chemical inhibitors to determine that

ligand binding drives proteolytic degradation *in vivo*, the first demonstration of LuxR/HapR function connected to ligand binding for this historical protein family.

INTRODUCTION

Vibrio species are Gram-negative, motile, facultatively anaerobic bacteria belonging to the family *Vibrionaceae* in the phylum Proteobacteria (Singleton et al., 1983). These bacteria are associated with a variety of marine organisms like corals, fish, shrimp, and zooplankton. Although some interactions are hypothesized to be commensal, several species are known pathogens of fish, coral, and shellfish(Fadel & El-Lamie, 2019; Guillemette et al., 2020; Halpern & Izhaki, 2017; Jayasree et al., 2006; Kemp et al., 2018; Paranjpye & Strom, 2005; Soto-Rodriguez et al., 2015; Thompson et al., 2004; Yang et al., 2017). Notably, at least 12 species in the genus *Vibrio* are pathogenic to humans, *i.e*., *V. cholerae*, *V. parahaemolyticus*, and *V. vulnificus* (Baker-Austin et al., 2018). Among these, *V. vulnificus* is a potent human pathogen with a mortality rate of >50% in primary septicemia infections (Jones & Oliver, 2009). Historically, infections were endemic to equatorial regions but due to a global rise in temperatures, there has been an alarming increase and spread of vibriosis to regions beyond their typical equatorial habitats(Coly et al., 2013; Le Roux et al., 2015; Martinez-Urtaza et al., 2013). This has consequently caused great harm to aquaculture industries, natural marine ecosystems, and human health worldwide(Froelich & Daines, 2020; Newton et al., 2012; Vezzulli et al., 2016; Jutla et al.,2011). Additionally, vibrios have been shown to evolve by gaining fitness traits through horizontal gene transfer (HGT), including genes encoding multidrug resistance(Mohan Raj et al., 2019; Verma et al., 2019). The emergence of multidrug resistant strains has prompted a need to develop alternative strategies to treat vibriosis.

In *Vibrio* species, one major regulatory system that controls expression of virulence genes is quorum sensing (QS), a cell-to-cell signaling system that allows bacteria to control group behaviors in response to alterations in population density(C. Fuqua et al., 1996; W. C. Fuqua et al., 1994; Waters et al., 2005). At low cell density, autoinducer concentrations are low, and multiple unbound receptors act as kinases to phosphorylate LuxU, the phosphotransfer protein. LuxU phosphorylates the response regulator LuxO, which, upon phosphorylation and together with σ-54, activates expression of the five Qrr sRNAs(Tu & Bassler, 2007). These repress the master QS transcription factor, a family of proteins only found in *Vibrios* and collectively called LuxR/HapR(Ball et al., 2017). The Qrrs also activate translation of the low cell density

regulator AphA, leading to expression of genes for individual behaviors (Rutherford et al., 2011; Van Kessel et al., 2013) (**Fig. S1**; model depicts *Vibrio campbellii* signaling system). At high cell density, binding of autoinducers and/or nitric oxide(B. Henares et al., 2013; B. M. Henares et al., 2012) to the receptors changes their activities to those of phosphatases, resulting in dephosphorylated LuxO and reduced Qrr expression. Thus, production of LuxR/HapR is highest at high cell density, and this master transcription factor regulates the expression of genes encoding for proteins with various functions(van Kessel et al., 2013a, 2013b, Chaparian et al., 2016). The master QS transcriptional regulators in each *Vibrio* species, *e.g.*, *V. campbellii* LuxR, *V. cholerae* HapR, and *V. vulnificus* SmcR, are highly conserved in pathogenic vibrios and are the central regulators of virulence gene expression(Ball et al., 2017; Barrasso et al., 2020). Importantly, these proteins are not at all similar to the LuxR-type proteins found associated with LuxI in other Gram-negative bacterial QS systems. Rather, the master QS transcription factors that we discuss here called the LuxR/HapR group are part of the broad TetR family of proteins. TetR proteins are characterized by dimeric complexes with an N-terminal helix-turn-helix DNA binding domain (DBD) and a C-terminal dimerization domain with a putative ligand-binding pocket (LBP), which typically mediates the conformation of the (DBD). Thus, TetR DNA-binding activity is typically controlled in a ligand-dependent manner (Cuthbertson & Nodwell, 2013). Crystal structures of SmcR and HapR revealed a putative l (LBP) near the dimerization domain that is characterized by hydrophobic residues and is hypothesized to contain an unidentified native ligand(R. S. De Silva et al., 2007; Y. Kim et al., 2010). However, no ligand has been identified to date. Thus, functional studies of the LuxR/HapR family of proteins and their ligand binding partners have been limited.

Because LuxR/HapR proteins are the central regulators of QS signaling genes, they have been a focus of research since their discovery(Swartzman et al., 1992). Indeed, their importance in *Vibrio* virulence gene regulation is well-documented; deletion of *smcR* or inhibition of SmcR in *V. vulnificus* decreases pathogenesis in both mouse and shrimp models(B. S. Kim et al., 2018; S. M. Kim et al., 2013). Recent studies have shown that QS inhibitors are feasible alternatives to traditional antibiotics with demonstrated efficacy in infection models (Jiang et al., 2019; Rémy et al., 2018). Because these inhibitors do not affect bacterial viability, they are hypothesized to generate less selective pressure for evolving resistance (Guendouze et al., 2017; Starkey et al., 2014). LuxR/HapR-specific inhibitors have been identified via *in vitro* and *in silico* screening efforts and include molecules with functional groups such as aromatic sulfonamides, enones, sulfones, furanones, brominated thiophenones, and cinnamaldehydes (Brackman et al., 2008, 2011; Defoirdt et al., 2007, 2012; Rajamanikandan et al., 2017a, 2017b;

Kim et al., 2020). Each of these specifically inhibits QS phenotypes in *V. campbellii* and/or other *Vibrio* species. However, most of these either did not result in significant inhibition of QS or required high concentrations to be effective. Kim *et. al.* identified a selective *Vibrio* QS inhibitor named Qstatin [1-(5-bromothiophene-2-sulfonyl)-1H-pyrazole], which inhibits *V. vulnificus* SmcR (B.S. Kim et al., 2018). Based on biochemical assays, they hypothesized that Qstatin binds to the putative LBP in SmcR, changing the entropic and enthalpic components of the system and altering SmcR regulatory activity *in vivo*. Their data showed that Qstatin resulted in complete SmcR dysfunction, eliminating the expression of the SmcR regulon required for virulence, biofilm dynamics, and motility/chemotaxis. Qstatin markedly attenuated different representative QS-regulated phenotypes in the test *Vibrio* species, including virulence against the brine shrimp (*Artemia franciscana*). However, the mechanism of action of Qstatin was not clear; addition of Qstatin did not alter DNA binding more than 2-fold *in vitro* (B.S. Kim et al., 2018), and this result was not observed in subsequent DNA binding assays (Newman, Russell, et al., 2021).

Subsequently, our group synthesized a panel of thiophenesulfonamide inhibitors and screened them for their inhibitory activity against different LuxR/HapR proteins. We identified several compounds that displayed equal or better efficacy compared to Qstatin against LuxR/HapR homologues in various *Vibrio* species with no impact on bacterial viability (Newman, Chopra, et al., 2021). From that panel, PTSP (3-**p**henyl-1-(**t**hiophen-2-yl**s**ulfonyl)-1*H*-**p**yrazole) was the most effective inhibitor (**Fig. 1A).** It inhibited the LuxR/HapR homologues in different *Vibrio* species at nanomolar to micromolar concentrations with distinct efficacies based on their respective putative LBP. Interestingly, PTSP showed strongest inhibition of *V. vulnificus* SmcR but did not inhibit *V. cholerae* HapR. Based on these results, the Raychaudhuri lab sought to determine the molecular basis of HapR insensitivity to Qstatin and its derivatives (Sen et al., 2023). They constructed a variant HapR by replacing four native LBP residues with SmcR residues, two of which our group had shown to be necessary for SmcR sensitivity to PTSP. They made single, double, triple, and quadruple substitution mutants at residues Y76F, L97I, I141V and F171C (Newman, Chopra, et al., 2021; Sen et al., 2023). Their assays showed that only the quadruple mutant was susceptible to Qstatin and its phenyl derivative inhibitor called IMT-VC-212 (Sen et al., 2023).

Here, we used a genetic screen and X-ray crystallography to examine PTSP interactions with SmcR. Our results show that multiple residues in the LBP of SmcR are critical for PTSP binding *in vivo*. Substitutions at residues in the LBP abrogate PTSP inhibition and restore wild-type activity to SmcR *in vivo*. PTSP binding to SmcR increases protein degradation by the ClpAP protease *in vivo*; SmcR variants that are resistant to PTSP were not susceptible to this

degradation. Thus, the mechanism of thiophenesulfonamide inhibition of SmcR is driven by proteolysis *in vivo*, indicating that the stability of SmcR, and possibly its conformation, is connected to interactions with the compound in its LBP.

RESULTS

Forward genetic screen identifies *smcR* alleles resistant to PTSP

Our previous study showed that substitutions F75Y or C170F rendered SmcR resistant to PTSP, whereas I96L and V140I did not affect PTSP sensitivity nor function (Newman, Chopra, et al., 2021). However, this was a limited reverse genetics experiment that encompassed only four substitutions in the putative LBP and did not determine if other residues are also involved in binding to ligand. To determine which SmcR residues are important for PTSP binding, we used a forward genetics approach in which we generated a *smcR* mutant library using error-prone PCR random mutagenesis. The mutant libraries were assayed in a previously established dual-reporter bioassay in *E. coli* that contains promoters from *V. campbellii* that are activated or repressed by LuxR/HapR-type proteins: 1) an activated reporter cassette comprising the *luxCDABE* promoter driving *gfp* expression, and 2) a repressed reporter cassette comprising the *05222* promoter driving *mCherry* expression (**Fig. 1B**) (van Kessel et al., 2013). Thus, in cells expressing wild-type *smcR*, GFP expression is high and mCherry expression is low. Conversely, in SmcR-expressing cells in the presence of PTSP, GFP expression is low and mCherry expression is high, mimicking cells that do not express *smcR* (**Fig. 1C, 1D**). As with our previous reverse genetics assay, we sought to identify mutant *smcR* alleles that were resistant to PTSP and expressed GFP and mCherry at levels comparable to wild-type *smcR* cells in media without PTSP. Using flow cytometry, we sorted PTSP-treated cells based on their GFP and mCherry expression profiles into high, moderate, and low resistance classes (**Fig. 1C, 1D**). From ~60,000 mutant alleles, we identified multiple isolates with mutant *smcR* alleles with substitutions at residues F75, F78, I96, M100, Q137, F166, H167, C170 and R179 (**Fig. 1C, 1D, Fig. S2**).

To assess the effect of substitutions in SmcR on QS regulation and growth, we focused on three PTSP-resistant *smcR* alleles resulting in substitutions at H167, C170 and R179 and constructed isogenic mutant *V. vulnificus* strains. *V. vulnificus* utilizes various virulence factors, such as exotoxins and other biofilm-related factors for its persistence in the environment and pathogenesis during infection (Choi & Choi, 2022). We examined the effect of PTSP on protease activity, a virulence factor that is known to be activated at high cell density by SmcR activation

of the *vvpE* gene (Jeong et al., 2003). We hypothesized that the resistant mutant strains would exhibit no change in protease activity in the presence of PTSP but expected protease activity to decrease or be eliminated upon PTSP binding in the wild-type strain. First, we measured each strain for growth and observed that the mutations did not lead to significant growth attenuation either in the presence or absence of PTSP (**Fig. S3**). We next measured protease activity in *V. vulnificus* supernatants using an azocasein-based assay. We observed that protease activity in wild-type *V. vulnificus* decreased ~10-fold upon treatment with 25 µm PTSP (**Fig. 1E**). Mutant strains treated with PTSP exhibited similar protease activities to the untreated cultures; although there were slight decreases in protease activity for each mutant, the only significant difference was in the strain expressing the SmcR variant R179C. We note that the protease activity of this mutant strain is significantly increased compared to wild-type in the untreated cultures, indicating that this substitution somehow alters basal SmcR activity. From these data, we conclude that we have identified mutants of *smcR* that render SmcR resistant to PTSP and maintain and/or increase SmcR activity *in vivo*.

PTSP binds to SmcR in the LBP

We used X-ray crystallography to determine the structural basis for the SmcR-PTSP interaction. We note that initial attempts to soak PTSP into already-formed SmcR protein crystals did not result in electron density maps that contained density consistent with a bound PTSP molecule, which was the method performed for the SmcR-Qstatin structure published (B. S. Kim et al., 2018). Instead, we added PTSP at the time of protein induction and screened for conditions that could promote crystallization of SmcR pre-bound to PTSP. We determined the structure of full-length SmcR bound to PTSP at 2.1 Å using molecular replacement (**Fig. 2A**; **Table S1; Movie S1**). The N-terminal DBD was largely disordered and residues 1-15 could not be modeled with high confidence and, thus, were not included in our final model (**Fig. S4A**). Additionally, the B-factors were high for residues in the more ordered region of the N-terminus (residues 16-62) that could be modeled compared to the rest of the structure (**Fig. S4A**). Indeed, it is possible this region of protein is actively unfolded or destabilized by the presence of PTSP, a point we address in our biochemical analyses of the SmcR-PTSP complex. Conversely, the C-terminal domain, which contains the putative LBP, was well-ordered and allowed for the unambiguous placement of PTSP (**Fig. 2B, Fig. S4B**). The putative LBP is bipartite with distinct hydrophobic and hydrophilic regions, similar to what is observed in the ligand binding domains of LuxR-type proteins (McCready et al., 2019). One-half of the LBP is comprised of hydrophobic residues (F75, F78, L79, I96, M100, W114, F115, V140, F166,

C170), which can accommodate the phenyl and pyrazole rings of PTSP (**Fig. 2B**). Additionally, the region of the LBP adjacent to the solvent accessible channel that allows for ligand accessibility to the binding site is lined with hydrophilic residues, which can act as a shield for the surrounding bulk solvent. Interestingly, residue R179 from one monomer of SmcR contacts water residues in the accessible ligand channel of the opposing monomer, potentially acting as a gate for ligand binding (**Fig. 2B; Fig. S4C)**. Furthermore, hydrophilic residues (N133, Q137, N164, H167) also contact water molecules and the thiophene head group of PTSP (**Fig. 2B**). In particular, residue N133 forms an important hydrogen bond with the sulfonyl group in PTSP (**Fig. 2B**). Nine of these residues were discovered as being important for binding to PTSP in our forward genetic screen of SmcR or through reverse genetics (Newman, Chopra, et al., 2021) (**Fig. 1B, 1C, S4**), lending validity to our model. Previous work in our lab revealed that HapR from *V. cholerae* was resistant to PTSP. To understand the molecular basis for the selectivity of SmcR for PTSP, we compared the LBP of SmcR to HapR. The most significant difference between the structures is at residues C170 in SmcR and F171 in HapR (**Fig. S4D**). When the PTSP-bound structure of SmcR and the apo structure of HapR were overlayed, residue F171 from HapR overlapped with the phenyl ring in PTSP, revealing a significant steric clash that would prevent PTSP binding to HapR (**Fig. S4D**).

In recent years, SmcR and HapR have been targets for small molecule modulation for QS-dependent repression of virulence. SmcR and HapR variants bound to molecules possessing similar moieties to PTSP have been solved, allowing us to determine the mechanism driving receptor inactivation. In Fig. 2C, we overlayed the structures of SmcR-apo, SmcR-Qstatin, HapR (Y76F, L97I, I141V and F171C)-IMT-VC-212 with a focus on the DBD of the receptors, specifically residue N55 in SmcR (N56 in HapR), which we previously showed to be important for recognizing DNA to initiate transcription (Newman, Russell, et al., 2021). Typical of TetR receptors, SmcR and HapR both have an extended α-helix (residues 60-84) that connects the putative LBP and the DBD. In the SmcR-PTSP structure, the first α-helix of the DBD is largely disordered, resulting in a displacement of N55, allowing the residue to point inward toward the core of the DBD rather than the bulk solvent (**Fig. 2C**; **Fig. S4E**). Collectively, from these data, we conclude that PTSP forms specific interactions with the LBP of SmcR, and alterations of the DBD conformation, at the α-carbon backbone level, are observed in the PTSP-bound structure compared to the apo-SmcR structure. However, due to the nature of the disordered N-terminus, we cannot reliably determine the specific molecular interactions that might drive such a change.

PTSP promotes SmcR flexibility in solution

To assess the potential conformational changes induced by PTSP binding in solution, we performed small-angle X-ray scattering (SAXS) experiments using SmcR-apo and SmcR-PTSP (**Fig. S5 and S6**). Consistent with previous work (Newman, Russell, et al., 2021), SAXS data collected for SmcR-apo fit well to high-resolution X-ray structure data (PDB: 6WAE) (low χ^2, with a value of 0.80. We observed a poor fit of the SmcR-PTSP SAXS data to high-resolution data, with a χ^2 value of 2.58 (**Fig. S7**, **Table S2**). This observation agrees with our X-ray crystallographic data, in which we observed disordered regions in the N-terminal DBD in the presence of PTSP. We hypothesized that these disordered regions are indicative of partial protein unfolding. The SAXS data revealed that SmcR-apo adopted a radius of gyration (R_g) of 28.6 Å, whereas SmcR-PTSP adopted a R_g of 30.4 Å. R_g is defined as the root mean squared deviation of the average of the distance of all electrons from the center of a particle as extrapolated from a Guinier plot of the raw data at low angles. Thus, apo-SmcR adopts a more compact shape compared to SmcR-PTSP, which has a more flexible structure in solution. Consistent with this, the pair-distance distribution functions derived from the scattering profiles, which is a calculation of the distance between any two atoms in a given volume, revealed an apo-SmcR profile with a bell-shaped curve and a single peak of a P(r)/I(0) ratio of 0.00175 at a distance of ~35 Å, resembling a globular protein with a compact shape. In contrast, the SmcR-PTSP scattering profile showed a smaller peak (P(r)/I(0) ratio of 0.00150) at a distance of ~35 Å, with an elongated that extended to higher r values, suggesting a flexible region of the protein and a potential conformational change in solution (**Fig. S7, Table S2)**. Overall, these data suggest that SmcR in the presence of PTSP undergoes partial unfolding in solution as compared to SmcR-apo.

Binding of PTSP increases SmcR thermostability *in vitro*

Based on our observations that SmcR bound to PTSP resulted in a disordered N-terminus spanning residues 1-50, we hypothesized that binding of PTSP to SmcR alters the conformation of the DNA binding domains. This is a commonly observed conformational change in TetR family proteins that are known to exhibit DNA binding domain movements as large as 10 Å (Werten et al., 2023). Although the apo-SmcR and SmcR-PTSP structures do not appear to have this large of a conformational change (**Fig. 2C**), we hypothesize that other alterations may exist that involve a destabilization of the DBD. Indeed, it is formally possible that both SmcR-apo and SmcR-PTSP are capable of binding DNA with equal affinity because the DBD of SmcR-PTSP can refold or reorient itself in the presence of high affinity DNA sites. To assess

the effect of PTSP binding on the SmcR quaternary structure in solution, we performed thermal shift assays to examine the melting profile of SmcR in the presence and absence of PTSP. This assay measures protein denaturation *in vitro* by tracking binding of fluorescent SYPRO Orange dye throughout an increasing heat curve; the dye binds to hydrophobic residues that become exposed as the protein unfolds. We measured unfolding of wild-type and SmcR variants in their apo form with or without the addition of PTSP to the reaction. We also compared these apo profiles to SmcR proteins that were purified in the presence of PTSP and then subsequently incubated with PTSP or the DMSO solvent control. The median melting temperature of wild-type SmcR in its apo form increased 5.0 °C in the presence of PTSP compared to the DMSO control, whereas there was no significant change in melting temperature when SmcR was purified pre-bound to PTSP in the presence of PTSP compared to the DMSO control. (**Fig. 3A, 3B, Table S3**). We next assayed a PTSP-resistant variant of SmcR. Based on our finding that certain SmcR variants are resistant to PTSP *in vivo*, we hypothesized that these mutants do not bind PTSP and thus would not display altered denaturation profiles either in the presence or absence of PTSP in the assay or prior to purification. As expected, we observed similar thermal shift profiles for SmcR C170F under all conditions tested, although the overall thermostability of this mutant protein is decreased compared to wild-type SmcR (**Fig. 3A, 3B, Table S3**). From these results, we conclude that PTSP binding increases the overall thermostability of SmcR *in vitro*. Further, mutation of SmcR C170F increases thermostability to a similar level as wild-type SmcR bound and/or incubated with PTSP.

PTSP increases proteolytic degradation of SmcR *in vivo*

From our structural and genetic experiments, we established that PTSP interacts with SmcR by binding in its LBP. Our mutational analyses identified gain-of-function mutants of SmcR that were resistant to PTSP activity *in vivo*. We hypothesized that this resistance phenotype was due to decreased or eliminated PTSP binding. However, this phenotype could also be due to increased expression of mutant SmcR proteins compared to wild-type SmcR. Thus, we examined SmcR protein expression in strains expressing wild-type and mutant *smcR* alleles in isogenic *V. vulnificus* mutant strains by western blot analysis. In the wild-type strain, we observed a clear reduction of SmcR protein levels in the presence of PTSP (**Fig. 4A**). Conversely, mutant strains expressing SmcR R179C, SmcR H167Q, and SmcR C170F variants did not show altered expression levels of these proteins with or without PTSP added (**Fig. 4A, 4B, 4C**). However, each variant assayed showed overall increased expression compared to wild-type SmcR regardless of the presence or absence of PTSP (**Fig. 4A, 4B, 4C**). We

observed the same results when measuring SmcR protein levels in the *E. coli* strains from the genetic screen (**Fig. S8**).

Next, we tested whether the decrease in SmcR levels upon PTSP addition was specific to this compound or a general effect of this panel of inhibitors. We assayed a select number of thiophenesulfonamide inhibitors that we previously synthesized and characterized *in vivo* (**Fig. 5A**). Each of the compounds tested resulted in a decrease in SmcR levels compared to the DMSO solvent control (**Fig. 5B**). For all compounds, the decreased levels of SmcR correlated with the inhibitor efficacy determined for *V. vulnificus in vivo*. For example, 10C and PTSP were the strongest inhibitors with the lowest IC_{50} (Newman, Chopra, et al., 2021)and also displayed the most severe decrease in SmcR levels *in vivo*. Conversely, 8A and 1A had comparatively lower efficacy and higher IC_{50} values against *V. vulnificus* SmcR, and the addition of these two compounds only moderately decreased SmcR levels (**Fig. 5B**).

To determine whether the decrease in protein levels upon addition of thiophenesulfonamides was specific to *V. vulnificus*, we assayed the same set of compounds in *V. campbellii* and *V. parahaemolyticus* and measured LuxR and OpaR levels, respectively. However, these endpoint assays did not reveal any detectable differences in LuxR/OpaR levels with or without addition of PTSP (**Fig. S9**). Thus, we used a modified assay to observe protein stability over time after translation is inhibited using chloramphenicol. With this assay, we observed qualitatively more SmcR protein degradation in *V. vulnificus* treated with PTSP compared to the DMSO control as early as 30 minutes post addition of chloramphenicol (**Fig. 6A**). Similarly, we observed degradation of LuxR in *V. campbellii* and OpaR in *V. parahaemolyticus* in cultures treated with PTSP compared to the DMSO controls. Over the four-hour time course, little degradation of SmcR/LuxR/OpaR was observed in the DMSO-treated cultures, supporting previous observations that these proteins are highly stable *in vivo* (van Kessel et al., 2013). From these results, we conclude that addition of thiophenesulfonamides results in degradation of SmcR/LuxR/OpaR protein levels *in vivo*. Further, we conclude that substitutions of specific PTSP-interacting residues stabilize and/or increase SmcR protein levels *in vivo*.

PTSP binding stimulates the ClpAP protease to degrade SmcR

SmcR and its homologue HapR have been shown to be degraded by the ClpAP protease *in vivo* (Andersson et al., 2009; Klancher et al., 2020; Lee et al., 2018). Further, SmcR is degraded by Lon protease under increased heat stress (Lee et al., 2018). Thus, we hypothesized that PTSP binding altered SmcR degradation by ClpAP and/or Lon proteases. To

test this, we assayed SmcR levels in wild-type, Δ*clpX*, Δ*clpA*, Δ*clpP*, and Δ*lon* mutant strains of *V. vulnificus* in the presence of PTSP or DMSO via western blot. First, we compared the levels of SmcR in the DMSO control and observed that SmcR was increased in Δ*clpA* and Δ*clpP* strains but levels were maintained in Δ*clpX* and Δ*lon* strains (**Fig. 7**), similar to what was observed for HapR in *V. cholerae* (Klancher et al., 2020). Next, we examined SmcR levels in the PTSP treatment compared to the DMSO control, and again we observed that wild-type SmcR decreased in the presence of PTSP, as well as in the Δ*clpX* and Δ*lon* strains. However, in the Δ*clpA* and Δ*clpP* strains, SmcR levels were similar with or without PTSP treatment (**Fig. 7**). This result suggests that SmcR is a substrate for the ClpAP protease, and binding of PTSP to SmcR makes it more susceptible to proteolytic cleavage by ClpAP. In total, our genetic, structural, and biochemical experiments have elucidated the mechanism of thiophenesulfonamide-driven inhibition of SmcR and its LuxR/HapR homologs.

Discussion

Vibrio species have served as cornerstone models for studying numerous bacterial behaviors, including biofilm formation, virulence factor secretion, host-pathogen interactions, bacteriophage-host evolution, signaling, and more (Fong et al., 2010; Higgins et al., 2007; A. J. Silva & Benitez, 2016; Visick, 2009;Murciano et al., 2015; Zamora-Pantoja et al., 2013; Kalatzis et al., 2018; Pollock et al., 2015; Wei et al., 2010).QS in particular was discovered in *Vibrio* species and much of the system knowledge in the field was established through research on QS in *Vibrio cholerae, Vibrio fischeri,* and *Vibrio campbellii* (in a strain previously classified as *V. harveyi*). The identification of the master transcriptional regulators at the center of the QS circuit that we call LuxR/HapR proteins led to the discovery of key gene families regulated by QS: biofilms, motility, competence, toxins, etc. The first structural assessment of this *Vibrio*-specific protein family focused on HapR, followed by similar studies of *V. vulnificus* SmcR and *V. alginolyticus* LuxR. The high amino acid identity of these proteins is even surpassed by the nearly identical tertiary structures of these proteins, which unsurprisingly bind to nearly identical DNA sequences *in vivo*. The literature is thorough in examinations of LuxR/HapR promoter DNA binding, gene regulons, and protein-protein interactions that drive the global activity of these proteins (Ball & van Kessel, 2019a; Chaparian et al., 2020; Rutherford et al., 2011; Zhang et al., 2021). However, one key attribute of these proteins has not been evaluated: the ligand binding potential. As a subset of the massive TetR protein family, LuxR/HapR proteins have a LBP clearly defined by an open channel lined with hydrophilic residues and a hydrophobic core (R. S. De Silva et al., 2007). Indeed, in every X-ray crystal structure of the “apo” protein, there is

density observed in the LBP, even though these proteins are purified from *E. coli*. Yet no phenotype has been determined for one of these proteins without its native ligand. Rather, a few studies have shown that inhibitors can bind LuxR/HapR proteins, decreasing their transcriptional regulation activity *in vivo*. Studies of thiophenesulfonamide inhibitors such as PTSP and Qstatin have likewise shown that these molecules bind specifically to LuxR/HapR proteins with varying affinities. However, the mechanism of action was not known. Assays *in vitro* for DNA binding yielded no significant differences in binding affinity, yet *in vivo* the addition of these compounds clearly blocked LuxR/HapR activity.

Here, we have identified the mechanism of thiophenesulfonamide inhibition of LuxR/HapR proteins, and we propose a model in **Figure 8**. Our data show that SmcR binds thiophenesulfonamides in its LBP, and addition of these compounds *in vitro* alters SmcR protein folding dynamics. We determined that thiophenesulfonamides such as PTSP drive SmcR proteolysis via the ClpAP protease, hence blocking its activity *in vivo*. Thus, we have uncovered the reason that *in vitro* DNA binding assays were not altered by addition of PTSP nor Qstatin but only *in vivo* activity was changed. Armed with this clear and measurable proteolysis phenotype driven by inhibitor binding, we now aim to uncover the role of the native ligand in LuxR/HapR function *in vivo*.

The next question we aim to focus on is: how does inhibitor binding to SmcR result in increased proteolysis? We hypothesize that this is accomplished via conformational changes, as is often observed with ligand binding for TetR proteins. Although we have successfully solved the structure of SmcR bound to PTSP, the structure itself does not indicate large conformational changes that might explain how SmcR is targeted for proteolysis when bound to PTSP. This may be due to the limited nature of X-ray crystallography in that the structures are not determined in solution, and not all possible conformations may form crystals. Based on our SAXS profiles and pair-distance distribution functions, SmcR bound to PTSP in solution adopts a more elongated and flexible conformation. This may be a potential mechanism for targeted proteolysis. Data from our thermal shift assays show that addition of PTSP to wild-type SmcR makes it more stable, suggesting that an allosteric effect on fold and/or tertiary structure. However, it is yet unclear if this change occurs in the DNA binding domain or elsewhere in the tertiary structure. We thus propose a model in which PTSP (or thiophenesulfonamides in general) binds to the LBP of each monomer in the LuxR/HapR protein, resulting in a conformational change that increases proteolysis of the dimer by the ClpAP protease (**Fig. 8**). We also aim to examine whether there is an adaptor protein such as ClpS required for proteolysis by ClpAP. Notably, the *clpS* mutant did not exhibit a change in HapR protein levels

in *V. cholerae*, suggesting ClpS is not required for ClpAP-mediated proteolysis in that system. Future genetic studies of the genes required for LuxR/HapR protein degradation and biochemical studies of ligand binding will inform the mechanism of thiophenesulfonamide-driven protein proteolysis.

Recent studies have shown that QS inhibitors are feasible alternatives to traditional antibiotics with demonstrated efficacy in infection models (Jiang et al., 2019; Rémy et al., 2018). As these inhibitors do not affect bacterial viability, they are hypothesized to generate less selective pressure for evolving resistance (Guendouze et al., 2017; Starkey et al., 2014). These factors make them attractive targets for *Vibrio* QS inhibition and possibly treatments for *Vibrio* diseases. For example, Qstatin markedly decreased virulence of three *Vibrio* species against the brine shrimp *A. franciscana*. Together, these results provide insights into the mechanism of action of an effective QS inhibitor that may be useful in controlling *Vibrio* virulence in aquaculture.

Methods

Bacterial strains and media

All strains and plasmids from this study are listed in Table S4 and Table S6. *Escherichia coli* strains DH10B and S17-1λpir were used for cloning, and BL21(DE3) was used for the overexpression of SmcR proteins. All *E. coli* strains and derivatives were grown at 30°C shaking at 275 rpm in Lysogeny Broth (LB) medium with appropriate antibiotics. *V. vulnificus*, *V. campbellii*, and *V. parahaemolyticus* strains and derivatives were grown shaking at 275 rpm at 30°C in LB Marine (LM) medium (LB with 2% NaCl final concentration) with appropriate antibiotics. Antibiotics were used at the following concentrations: kanamycin 40µg/ml or 100µg/ml (*E. coli* or *Vibrio*, respectively), chloramphenicol (10 µg/ml), and tetracycline (10 µg/ml).

Compound synthesis

Qstatin, PTSP, and all other derivatives used in this study were either synthesized as elaborated in Newman *et. al*, 2021.

Random mutagenesis and flow cytometry

The *smcR* mutant alleles were created using GeneMorph II EZClone Domain Mutagenesis Kit (Stratagene) as per the company protocol targeting the *smcR* gene encoded on plasmid pJN22,

which expresses *V. vulnificus smcR* under control of the IPTG-inducible P_{tac} promoter (Newman, Chopra, et al., 2021). Mutant libraries were transformed into S17-1λpir competent cells, pooled, and stored at -80°C. DNA was extracted from the library and then transformed into competent cells of *E. coli* strain DH10B containing the pJV064 reporter plasmid, selected on LB plates with kanamycin and chloramphenicol, pooled, and stored at -80°C. Overnight cultures of the pooled library were back-diluted 1:1,000 into fresh LB media with chloramphenicol (10µg/ml), kanamycin (40µg/ml) and IPTG (50 μm), treated with either DMSO or PTSP (25 μm) and grown shaking at 30°C overnight. Aliquots were prepared for flow cytometry by making 1:100 or 1:1,000 dilutions in PBS 30 mins prior to flow. Mutant strains resistant to PTSP were isolated by sorting cells with high GFP and low mCherry fluorescence on a FACS Aria II. Following sorting, colonies were inoculated individually into fresh medium, grown to stationary phase, and stored at -80°C.

Dual-reporter E. coli *bioassay*

Overnight *E. coli* cultures containing either pJN22 or empty vector control pMMB67EH-kanR and the pJV064 reporter were diluted 1:100 into LB with chloramphenicol (10 µg/ml) and kanamycin (40 µg/ml) and aliquoted into black-welled, clear-bottomed 96-well plates to a final volume of 150 µl. PTSP was resuspended in DMSO at a stock concentration of 10 mM and added to *E. coli* cultures at a final concentration of 25 µM unless otherwise stated. DMSO was added as a negative control at equal final concentration. 50 µM IPTG was also added to the wells to activate expression of *smcR*. The 96-well plates were covered in microporous sealing tape and grown for 16-18 hr shaking at 275 rpm at 30°C. The OD_{600} and GFP and mCherry fluorescence were measured on a BioTek Cytation plate reader.

Molecular methods

All PCR reactions were performed using Phusion HF polymerase (New England Biolabs). All oligonucleotides were purchased from Integrated DNA Technologies (IDT), and those used in this study are listed (Table S5). All mutant strains (Table S4) were confirmed by DNA sequencing (Eurofins). Cloning details are available upon request.

SmcR protein purification

His-tagged wild-type and mutant SmcR proteins were expressed and purified as described previously (Newman & van Kessel, 2021) using an Akta Pure L FPLC with His-Trap and gel-filtration columns. For induction of His-tagged wild-type and mutant His-SmcR in

presence of PTSP, induction media were supplemented with 50 μM of PTSP dissolved in DMSO. No additional PTSP was added to buffers during purification. Proteins were stored in gel filtration buffer (25 mM Tris, 300 mM NaCl, 1 mM DTT, 5 mM EDTA at pH 7.5) at 4°C.

Thermal shift assays

Wild-type or mutant purified protein preps of His-SmcR, induced with or without PTSP, were diluted to 5 μM in reaction buffer (20 mM Tris-HCl, pH 8, 200 mM NaCl, and 1 mM DTT) containing DMSO or 10 μM PTSP dissolved in DMSO in an 18-μl total volume and allowed to incubate at room temperature for 15 min. SYPRO Orange (5,000X) dissolved in DMSO was diluted to 200X in reaction buffer and used at 20X final concentration (2 μl added to each 18-μl reaction). 20-μl samples were assessed for thermal shifts in 96-well plates on a Quant Studio 6 Flex System (Applied Biosystems) using the melting curve setting and measuring fluorescence using the ROX reporter setting. Samples were incubated at 25°C for 2 min and then subjected to a linear gradient of 0.03°C/s until the temperature reached 99°C, where it was held for 2 min.

V. vulnificus strain construction

Isogenic strains containing mutations in *smcR* were generated by mutating wild-type *V. vulnificus* strain ATCC 27562. All isogenic mutant strains were generated using natural transformation via *tfoX* induction and MuGENT (A. B. Dalia, 2018; T. N. Dalia et al., 2017) via oligonucleotides listed in Table S5. First, derivative cas-vv006 was constructed in which a trimethoprim-resistance (Tm^R) cassette was inserted downstream of *smcR* at the native locus. The cas-vv006 strain was then used as a template to amplify *smcR*-Tm^R and generate targeting DNA to introduce substitutions into *smcR* via natural transformation. These DNA products were then introduced into wild-type *V. vulnificus* and selected for on LM plates with trimethoprim (10 μg/ml). All isogenic mutant strains were confirmed by sequencing at the *smcR* locus.

V. vulnificus growth curves

Vibrio strains were inoculated in 5 ml LM overnight at 30℃ shaking at 275 rpm with kanamycin (100 μg/ml), spectinomycin (200 μg/ml), or trimethoprim (10 μg/ml) to select for reporter plasmids. Overnight cultures were back-diluted 1:100,000 in LM with antibiotics, treated with 25 μm PTSP or equal volume of DMSO and transferred into clear-bottomed 96-well plate. The plate was covered and incubated in a BioTek Cytation plate reader overnight with shaking at 275 rpm at 37°C for 22 hr. OD_{600} was measured at 30 min intervals throughout the overnight incubation period.

Protease assays

Vibrio strains were inoculated in 5 ml LM with kanamycin (100 µg/ml), spectinomycin (200 µg/ml) or trimethoprim (10 µg/ml) and incubated overnight at 30°C shaking at 275 rpm. Overnight cultures were back diluted 1:1,000 in 10 ml LM with kanamycin (100 µg/ml), spectinomycin (200 µg/ml) or trimethoprim (10 µg/ml) and the cell mixture was equally aliquoted into test and control sets, with 5 ml culture per set. PTSP was added to test reactions at a concentration of 25 µM while DMSO was added as a negative control at equal final concentrations into control reactions. These cultures were grown for 16-18 hrs shaking at 275 rpm at 30°C. After incubation, OD_{600} was measured (1:10 dilution of overnights), and 1 ml of overnight undiluted cultures were pelleted in 1.7 ml micro centrifuge tube at 13,000 rpm for 10 min at room temperature. 100 µl supernatant was transferred to a new clear 1.7 ml microcentrifuge tube and incubated with 400 µL of 1% azocasein (0.01 mg/ml dissolved in dH_2O) for 2 hrs 30 min at 37°C. The reaction was stopped by addition of 600 µl 10% trichloroacetic acid, and the tubes were further incubated on ice for 30 min, then centrifuged at 13,000 rpm for 5 min at room temperature. 800 µl of the protease reaction was transferred to a new clear microcentrifuge tube, and 200 µl of 1.8 N NaOH was added. OD_{420} was measured in a desktop spectrophotometer. Protease activity was calculated by dividing OD_{420} by OD_{600}. Each assay was performed in technical and biological triplicates.

Western blots

Vibrio strains were inoculated in 5 ml LM with kanamycin (100 µg/ml), spectinomycin (200 µg/ml) or trimethoprim (10 µg/ml) and incubated overnight at 30°C or 42°C shaking at 275 rpm. Overnight cultures were back diluted 1:1,00 in 10 ml LM with kanamycin (100 µg/ml), spectinomycin (200 µg/ml) or trimethoprim (10 µg/ml) and the cell mixture was equally aliquoted into test and control sets, with 5 ml culture per set. PTSP was added to test reactions at a concentration of 25 µM while DMSO was added as a negative control at equal final concentrations into control reactions. These were incubated at 30°C shaking at 275 rpm overnight. Cells were harvested and resuspended in lysis buffer (1 ml Bugbuster (1X),5µl lysozyme (10 mg/ml,1µl Benzonase) to an OD_{600} of 0.005 and incubated at room temperature for 10 minutes. Western blot analyses were performed as previously described (van Kessel et al., 2013), except that new anti-LuxR antibodies were generated through Cocalico against purified LuxR protein. In addition, the western blots were probed with anti-RpoB as a loading control as previously described (Neoclone)(Ball & van Kessel, 2019b).

Purification of SmcR:PTSP for crystallographic studies

His-tagged WT SmcR-PTSP was expressed and purified via Ni-affinity chromatography as previously described. Induction of expression was performed in induction media supplemented with 50 µM PTSP in DMSO. Clarified cell lysates were incubated with Ni-NTA running buffer equilibrated NEBExpress Ni Resin for 1 hour with rocking at 4°C. Incubated resin was applied to a gravity column and washed with 100 mL Ni-NTA running buffer. His-tagged WT SmcR-PTSP was eluted in 10 mL Ni-NTA elution buffer in 1 mL fractions. Peak fractions, confirmed by SDS-PAGE, were pooled, and concentrated to 1 mL over a 10 kDa MWCO filter (Amicon) for injection on a Superdex-200 size exclusion column (Cytiva) equilibrated with gel-filtration buffer (25 mM Tris-HCl pH 7.5, 200 mM NaCl, 1 mM DTT). Peak fractions, determined by 280 nm absorbance and confirmed by SDS-PAGE, were pooled and concentrated to 5.2 mg/mL in gel-filtration buffer. SmcR:PTSP was stored at 4°C for immediate crystallographic screening.

Crystallographic studies

Previous crystallographic conditions for the determination of the SmcR-apo and SmcR-Qstatin structures did not yield crystals for SmcR-PTSP. Purified SmcR-PTSP (5.2 mg/mL) in gel-filtration buffer was screened using a variety of kit solutions (Nextal and Hampton) using a Gryphon Crystallization Robot (ART Robbins Instruments) and incubated at RT for 4 days. Optimization screens were performed using the hanging drop vapor diffusion method in 24-well crystallization trays. Initial SmcR-PTSP crystals were grown by mixing 1 µL protein solution with 1 µL well solution (2.0 M $MgSO_4$, 0.1 M MES pH 6.5) and sealed over a 1 mL well solution. After incubation for 24 hours at RT, SmcR-PTSP crystals were harvested, transferred to a PCR tube containing well solution, and vortexed. Fragmented crystals were used to streak-seed new drops of 1:1 protein:well solution to optimize crystal order and size. We thank Ted and Artemis Andrus-Paczkowski for the generous donation of their shed whiskers. Seeded SmcR-PTSP crystals formed after 24 hours incubating at RT, were batch harvested and soaked in cryoprotectant (20% v/v glycerol, 0.1 M MES pH 6.5, 1.6 M $MgSO_4$) for 10 min. After the cryoprotecting step, single crystals were mounted on a MiTeGen loop and flash frozen and stored under liquid nitrogen.

Data collection and structure solution

X-ray diffraction data were collected at Brookhaven National Laboratory National Synchrotron Light Source-II on the NYX beamline. Diffraction images were processed in XDS and data reduction was performed using CCP4-8.0.013 and Aimless. Automated and manual structure solutions were generated via molecular replacement using *MrBUMP* and *SHELXE-MR*, respectively. Molecular replacement in MrBUMP fit two copies of *V. vulnificus* SmcR-Qstatin (PDB: 5X3R, seq. identity 100%) chain A with waters, sulfate ions, and Qstatin removed. Results from MrBUMP were used for molecular replacement in SHELXE-MR. Alternating rounds of manual and automated refinement were performed using Coot v0.9.8.8 and REFMAC5. Structural validation was performed using Molprobity. Graphics were created using PyMol.

Small angle X-ray scattering

SAXS data were collected at the Cornell High Energy Synchrotron Source (CHESS) 7A1 beamline over multiple runs. For all runs, a 250 µM x 250 µM X-ray beam with a wavelength of 1.094 Å at 7.1×10^{11} photons s^{-1} was used and centered on a quartz capillary sample cell with a path length of 1.5 mm. 10, 1-second images were collected using a dual Pilatus 100K-S detector system (Dectris, Baden, Sweden), covering a range of $q \approx 0.0079$-0.45 $Å^{-1}$. The 1D SAXS profiles were grouped by sample and averaged, followed by buffer subtraction (25 mM Tris-HCl pH 7.5, 200 mM NaCl, and 1 mM DTT) within BioXTAS RAW (v2.2.1) (Hopkins et al., 2017). The radius of gyration (R_g) and forward scattering intensity $I(0)$ were estimated by Guinier fit analysis, and the pair distance distribution function analysis was done in GNOM (Svergun, 1992) utilizing the ATSAS software suite (Franke et al., 2017)(v3.2.1-1) implemented in BioXTAS RAW (Hopkins et al., 2017) (v2.2.1). The molecular weights were estimated in a concentration independent manner from the Porod volume, V_p (Piiadov et al., 2019). Single-state modelling was performed using the FoXS server (https://modbase.compbio.ucsf.edu/foxs/)(Schneidman-Duhovny et al., 2013, 2016).

Data analysis

All kinetic data were processed using GraphPad Prism software (GraphPad Software, Inc). For statistical significance tests, data were analyzed using GraphPad Prism to perform tests to conform the normal distribution of the data (Shapiro-Wilk) with subsequent parametric tests for significance (ANOVA and/or t-tests) as indicated in the figure legends.

Data availability

All data that support the conclusions of this study are contained or described within the text or supporting information. Bacterial strains, oligonucleotides, plasmids, compounds, or other reagents generated by this research study will be made available upon request to the corresponding author.

Conflict of interest

JVK and LCB disclose their relationship with company Quornix, LLC as board members and owners, and both JVK and LCB have a patent pending for thiophenesulfonamide compounds and their methods of use (application number 63/064,963). All other authors declare that they have no conflicts of interest.

Acknowledgments

We thank Dr. Giovanni Gonzalez-Gutierrez and Juan Nysschen at Indiana University for technical support, and Dr. Kyung-Jo Lee for sending us *V. vulnificus* ClpAP mutant strains. This research used resources of the National Synchrotron Light Source II (NSLS-II), a U.S. Department of Energy (DOE) Office of Science User Facility operated for the DOE Office of Science by Brookhaven National Laboratory under Contract NO. DE-SC0012704. The authors thank Kevin Battaile, Director of the NYX beamline at NSLS-II at Brookhaven National Laboratory, for technical assistance during data collection. We would like to thank the members of van Kessel lab for their support and thoughtful discussions. Cartoon diagrams in Figures S1 and 8 were created with Biorender.

Author contributions

JVK, JEP, LCB, and TR designed the research, TR, CPM, MWB, and JEP performed experiments, JVK, JEP, LCB, CPM, and TR analyzed data, and JVK, JEP, LCB, CPM, and TR wrote the manuscript.

Funding and additional information

The project was supported by NIH training grant T32GM132066 and NSF REU award DBI-175710 to MWB, NIH grant R01GM14436101 to JEP, and NIH grant R35GM124698 to JVK. This work is based on research conducted at the Center for High-Energy X-ray Sciences (CHEXS), which is supported by the National Science Foundation (BIO, ENG and MPS Directorates) under award DMR-1829070, and the Macromolecular Diffraction at CHESS (MacCHESS) facility, which is supported by award 1-P30-GM124166-01A1 from the National

Institute of General Medical Sciences, National Institutes of Health, and by New York State's Empire State Development Corporation (NYSTAR).

REFERENCES

Akanda, A. S., Griffiths, J. K., Colwell, R., Islam, S., & Jutla, A. S. (2011). Warming Oceans, Phytoplankton, and River Discharge: Implications for Cholera Outbreaks. *The American Journal of Tropical Medicine and Hygiene*, *85*(2), 303–308. https://doi.org/10.4269/ajtmh.2011.11-0181

Andersson, F. I., Tryggvesson, A., Sharon, M., Diemand, A. V., Classen, M., Best, C., Schmidt, R., Schelin, J., Stanne, T. M., Bukau, B., Robinson, C. V., Witt, S., Mogk, A., & Clarke, A. K. (2009). Structure and function of a novel type of ATP-dependent Clp protease. *Journal of Biological Chemistry*, *284*(20), 13519–13532. https://doi.org/10.1074/jbc.M809588200

Baker-Austin, C., Oliver, J. D., Alam, M., Ali, A., Waldor, M. K., Qadri, F., & Martinez-Urtaza, J. (2018). Vibrio spp. infections. *Nature Reviews Disease Primers*, *4*(1). https://doi.org/10.1038/s41572-018-0005-8

Ball, A. S., Chaparian, R. R., & Van Kessel, J. C. (2017). *Quorum Sensing Gene Regulation by LuxR/HapR Master Regulators in Vibrios*. https://doi.org/10

Ball, A. S., & van Kessel, J. C. (2019a). The master quorum-sensing regulators LuxR/HapR directly interact with the alpha subunit of RNA polymerase to drive transcription activation in *Vibrio harveyi* and *Vibrio cholerae*. *Molecular Microbiology*, *111*(5), 1317–1334. https://doi.org/10.1111/mmi.14223

Ball, A. S., & van Kessel, J. C. (2019b). The master quorum-sensing regulators LuxR/HapR directly interact with the alpha subunit of RNA polymerase to drive transcription activation in Vibrio harveyi and Vibrio cholerae. *Molecular Microbiology*, *111*(5), 1317–1334. https://doi.org/10.1111/mmi.14223

Barrasso, K., Watve, S., Simpson, C. A., Geyman, L. J., van Kessel, J. C., & Ng, W. L. (2020). Dual-function quorum-sensing systems in bacterial pathogens and symbionts. *PLoS Pathogens*, *16*(10). https://doi.org/10.1371/journal.ppat.1008934

Brackman, G., Celen, S., Hillaert, U., van Calenbergh, S., Cos, P., Maes, L., Nelis, H. J., & Coenye, T. (2011). Structure-activity relationship of cinnamaldehyde analogs as inhibitors of AI-2 based quorum sensing and their effect on virulence of Vibrio spp. *PLoS ONE*, *6*(1). https://doi.org/10.1371/journal.pone.0016084

Brackman, G., Defoirdt, T., Miyamoto, C., Bossier, P., Van Calenbergh, S., Nelis, H., & Coenye, T. (2008). Cinnamaldehyde and cinnamaldehyde derivatives reduce virulence in Vibrio spp. by decreasing the DNA-binding activity of the quorum sensing response regulator LuxR. *BMC Microbiology*, *8*. https://doi.org/10.1186/1471-2180-8-149

Chaparian, R. R., Ball, A. S., & van Kessel, J. C. (2020). Hierarchical Transcriptional Control of the LuxR Quorum-Sensing Regulon of Vibrio harveyi. *Journal of Bacteriology*, *202*(14). https://doi.org/10.1128/JB.00047-20

Chaparian, R. R., Olney, S. G., Hustmyer, C. M., Rowe-Magnus, D. A., & van Kessel, J. C. (2016). Integration host factor and LuxR synergistically bind DNA to coactivate quorum-sensing genes in Vibrio harveyi. *Molecular Microbiology*, *101*(5), 823–840. https://doi.org/10.1111/mmi.13425

Choi, G., & Choi, S. H. (2022). Complex regulatory networks of virulence factors in Vibrio vulnificus. *Trends in Microbiology*, *30*(12), 1205–1216. https://doi.org/10.1016/J.TIM.2022.05.009

726 Coly, I., Gassama Sow, A., Seydi, M., & Martinez-Urtaza, J. (2013). *Vibrio cholerae* and *Vibrio*
727 *parahaemolyticus* Detected in Seafood Products from Senegal. *Foodborne Pathogens and Disease*,
728 *10*(12), 1050–1058. https://doi.org/10.1089/fpd.2013.1523

729 Cuthbertson, L., & Nodwell, J. R. (2013). The TetR Family of Regulators. *Microbiology and Molecular*
730 *Biology Reviews*, *77*(3), 440–475. https://doi.org/10.1128/MMBR.00018-13

731 Dalia, A. B. (2018). *Natural Cotransformation and Multiplex Genome Editing by Natural Transformation*
732 *(MuGENT) of Vibrio cholerae* (pp. 53–64). https://doi.org/10.1007/978-1-4939-8685-9_6

733 Dalia, T. N., Hayes, C. A., Stolyar, S., Marx, C. J., McKinlay, J. B., & Dalia, A. B. (2017). Multiplex Genome
734 Editing by Natural Transformation (MuGENT) for Synthetic Biology in *Vibrio natriegens*. *ACS*
735 *Synthetic Biology*, *6*(9), 1650–1655. https://doi.org/10.1021/acssynbio.7b00116

736 Defoirdt, T., Benneche, T., Brackman, G., Coenye, T., Sorgeloos, P., & Scheie, A. A. (2012). A quorum
737 sensing-disrupting brominated thiophenone with a promising therapeutic potential to treat
738 luminescent vibriosis. *PLoS ONE*, *7*(7). https://doi.org/10.1371/journal.pone.0041788

739 Defoirdt, T., Miyamoto, C. M., Wood, T. K., Meighen, E. A., Sorgeloos, P., Verstraete, W., & Bossier, P.
740 (2007). The natural furanone (5Z)-4-bromo-5-(bromomethylene)-3-butyl-2(5H)-furanone disrupts
741 quorum sensing-regulated gene expression in Vibrio harveyi by decreasing the DNA-binding activity
742 of the transcriptional regulator protein luxR. *Environmental Microbiology*, *9*(10), 2486–2495.
743 https://doi.org/10.1111/j.1462-2920.2007.01367.x

744 De Silva, R. S., Kovacikova, G., Lin, W., Taylor, R. K., Skorupski, K., & Kull, F. J. (2007). Crystal structure of
745 the Vibrio cholerae quorum-sensing regulatory protein HapR. *Journal of Bacteriology*, *189*(15),
746 5683–5691. https://doi.org/10.1128/JB.01807-06

747 Fadel, H. M., & El-Lamie, M. M. M. (2019). Vibriosis and Aeromonas infection in shrimp: Isolation,
748 sequencing, and control. *International Journal of One Health*, *5*, 38–48.
749 https://doi.org/10.14202/IJOH.2019.38-48

750 Fong, J. C. N., Syed, K. A., Klose, K. E., & Yildiz, F. H. (2010). Role of Vibrio polysaccharide (vps) genes in
751 VPS production, biofilm formation and Vibrio cholerae pathogenesis. *Microbiology*, *156*(9), 2757–
752 2769. https://doi.org/10.1099/mic.0.040196-0

753 Franke, D., Petoukhov, M. V., Konarev, P. V., Panjkovich, A., Tuukkanen, A., Mertens, H. D. T., Kikhney, A.
754 G., Hajizadeh, N. R., Franklin, J. M., Jeffries, C. M., & Svergun, D. I. (2017). *ATSAS 2.8*: a
755 comprehensive data analysis suite for small-angle scattering from macromolecular solutions.
756 *Journal of Applied Crystallography*, *50*(4), 1212–1225.
757 https://doi.org/10.1107/S1600576717007786

758 Froelich, B. A., & Daines, D. A. (2020). In hot water: effects of climate change on Vibrio–human
759 interactions. In *Environmental Microbiology* (Vol. 22, Issue 10, pp. 4101–4111). Blackwell
760 Publishing Ltd. https://doi.org/10.1111/1462-2920.14967

761 Fuqua, C., Winans, S. C., & Greenberg, E. P. (1996). CENSUS AND CONSENSUS IN BACTERIAL
762 ECOSYSTEMS: The LuxR-LuxI Family of Quorum-Sensing Transcriptional Regulators. *Annual Review*
763 *of Microbiology*, *50*(1), 727–751. https://doi.org/10.1146/annurev.micro.50.1.727

764 Fuqua, W. C., Winans, S. C., & Peter Greenberg2, E. (1994). MINIREVIEW Quorum Sensing in Bacteria:
765 the LuxR-LuxI Family of Cell Density-Responsive Transcriptional Regulatorst. In *JOURNAL OF*
766 *BACTERIOLOGY* (Vol. 176, Issue 2).

767 Guendouze, A., Plener, L., Bzdrenga, J., Jacquet, P., Rémy, B., Elias, M., Lavigne, J. P., Daudé, D., &
768 Chabrière, E. (2017). Effect of quorum quenching lactonase in clinical isolates of pseudomonas
769 aeruginosa and comparison with quorum sensing inhibitors. *Frontiers in Microbiology*, *8*(FEB).
770 https://doi.org/10.3389/fmicb.2017.00227

771 Guillemette, R., Ushijima, B., Jalan, M., Häse, C. C., & Azam, F. (2020). Insight into the resilience and
772 susceptibility of marine bacteria to T6SS attack by Vibrio cholerae and Vibrio coralliilyticus. *PLoS*
773 *ONE*, *15*(1). https://doi.org/10.1371/journal.pone.0227864

774 Halpern, M., & Izhaki, I. (2017). Fish as hosts of Vibrio cholerae. In *Frontiers in Microbiology* (Vol. 8, Issue
775 FEB). Frontiers Research Foundation. https://doi.org/10.3389/fmicb.2017.00282

776 Henares, B. M., Higgins, K. E., & Boon, E. M. (2012). Discovery of a Nitric Oxide Responsive Quorum
777 Sensing Circuit in *Vibrio harveyi*. *ACS Chemical Biology*, *7*(8), 1331–1336.
778 https://doi.org/10.1021/cb300215t

779 Henares, B., Xu, Y., & Boon, E. (2013). A Nitric Oxide-Responsive Quorum Sensing Circuit in Vibrio
780 harveyi Regulates Flagella Production and Biofilm Formation. *International Journal of Molecular*
781 *Sciences*, *14*(8), 16473–16484. https://doi.org/10.3390/ijms140816473

782 Higgins, D. A., Pomianek, M. E., Kraml, C. M., Taylor, R. K., Semmelhack, M. F., & Bassler, B. L. (2007).
783 The major Vibrio cholerae autoinducer and its role in virulence factor production. *Nature*,
784 *450*(7171), 883–886. https://doi.org/10.1038/nature06284

785 Jayasree, L., Janakiram, P., & Madhavi, R. (2006). *Characterization of Vibrio spp. Associated with*
786 *Diseased Shrimp from Culture Ponds of Andhra Pradesh (India).*

787 Jeong, H. S., Lee, M. H., Lee, K.-H., Park, S.-J., & Choi, S. H. (2003). SmcR and Cyclic AMP Receptor Protein
788 Coactivate Vibrio vulnificus vvpE Encoding Elastase through the RpoS-dependent Promoter in a
789 Synergistic Manner. *Journal of Biological Chemistry*, *278*(46), 45072–45081.
790 https://doi.org/10.1074/jbc.M308184200

791 Jiang, Q., Chen, J., Yang, C., Yin, Y., Yao, K., & Song, D. (2019). Quorum Sensing: A Prospective
792 Therapeutic Target for Bacterial Diseases. In *BioMed Research International* (Vol. 2019). Hindawi
793 Limited. https://doi.org/10.1155/2019/2015978

794 Jones, M. K., & Oliver, J. D. (2009). Vibrio vulnificus: Disease and pathogenesis. In *Infection and Immunity*
795 (Vol. 77, Issue 5, pp. 1723–1733). https://doi.org/10.1128/IAI.01046-08

796 Kalatzis, P., Castillo, D., Katharios, P., & Middelboe, M. (2018). Bacteriophage Interactions with Marine
797 Pathogenic Vibrios: Implications for Phage Therapy. *Antibiotics*, *7*(1), 15.
798 https://doi.org/10.3390/antibiotics7010015

799 Kemp, K. M., Westrich, J. R., Alabady, M. S., Edwards, M. L., & Lipp, E. K. (2018). Abundance and
800 multilocus sequence analysis of Vibrio bacteria associated with diseased elkhorn coral (Acropora

801 palmata) of the Florida Keys. *Applied and Environmental Microbiology*, *84*(2).
802 https://doi.org/10.1128/AEM.01035-17

803 Kim, B. S., Jang, S. Y., Bang, Y. J., Hwang, J., Koo, Y., Jang, K. K., Lim, D., Kim, M. H., & Choi, S. H. (2018).
804 QStatin, a selective inhibitor of quorum sensing in Vibrio species. *MBio*, *9*(1).
805 https://doi.org/10.1128/mBio.02262-17

806 Kim, S. M., Park, J. H., Lee, H. S., Kim, W. Bin, Ryu, J. M., Han, H. J., & Choi, S. H. (2013). LuxR Homologue
807 SmcR Is Essential for Vibrio vulnificus Pathogenesis and Biofilm Detachment, and Its Expression is
808 Induced by Host Cells. *Infection and Immunity*, *81*(10), 3721–3730.
809 https://doi.org/10.1128/IAI.00561-13

810 Kim, S. M., Park, J., Kim, M. S., Song, H., Jo, A., Park, H., Kim, T. S., Choi, S. H., & Park, S. B. (2020).
811 Phenotypic Discovery of an Antivirulence Agent against Vibrio vulnificus via Modulation of
812 Quorum-Sensing Regulator SmcR. *ACS Infectious Diseases*, *6*(11), 3076–3082.
813 https://doi.org/10.1021/acsinfecdis.0c00587

814 Kim, Y., Kim, B. S., Park, Y. J., Choi, W. C., Hwang, J., Kang, B. S., Oh, T. K., Choi, S. H., & Kim, M. H. (2010).
815 Crystal structure of SmcR, a quorum-sensing master regulator of Vibrio vulnificus, provides insight
816 into its regulation of transcription. *Journal of Biological Chemistry*, *285*(18), 14020–14030.
817 https://doi.org/10.1074/jbc.M109.100248

818 Klancher, C. A., Newman, J. D., Ball, A. S., Van Kessel, J. C., & Dalia, A. B. (2020). *Species-Specific Quorum*
819 *Sensing Represses the Chitobiose Utilization Locus in Vibrio cholerae*. https://doi.org/10

820 Lee, K. J., Jung, Y. C., Park, S. J., & Lee, K. H. (2018). Role of heat shock proteases in quorum-sensing-
821 mediated regulation of biofilm formation by Vibrio species. *MBio*, *9*(1).
822 https://doi.org/10.1128/mBio.02086-17

823 Le Roux, F., Wegner, K. M., Baker-Austin, C., Vezzulli, L., Osorio, C. R., Amaro, C., Ritchie, J. M., Defoirdt,
824 T., Destoumieux-Garzón, D., Blokesch, M., Mazel, D., Jacq, A., Cava, F., Gram, L., Wendling, C. C.,
825 Strauch, E., Kirschner, A., & Huehn, S. (2015). The emergence of Vibrio pathogens in Europe:
826 Ecology, evolution and pathogenesis (Paris, 11-12 March 2015). *Frontiers in Microbiology*, *6*(JUL).
827 https://doi.org/10.3389/fmicb.2015.00830

828 Martinez-Urtaza, J., Baker-Austin, C., Jones, J. L., Newton, A. E., Gonzalez-Aviles, G. D., & DePaola, A.
829 (2013). Spread of Pacific Northwest Vibrio parahaemolyticus Strain . *New England Journal of*
830 *Medicine*, *369*(16), 1573–1574. https://doi.org/10.1056/nejmc1305535

831 McCready, A. R., Paczkowski, J. E., Henke, B. R., & Bassler, B. L. (2019). Structural determinants driving
832 homoserine lactone ligand selection in the Pseudomonas aeruginosa LasR quorum-sensing
833 receptor. *Proceedings of the National Academy of Sciences of the United States of America*, *116*(1),
834 245–254. https://doi.org/10.1073/pnas.1817239116

835 Mohan Raj, J., Vittal, R., Shivakumaraswamy, S., Deekshit, V., Chakraborty, A., & Karunasagar, I. (2019).
836 Presence & mobility of antimicrobial resistance in Gram-negative bacteria from
837 environmental samples in coastal Karnataka, India. *Indian Journal of Medical Research*, *149*(2), 290.
838 https://doi.org/10.4103/ijmr.IJMR_2088_17

Murciano, C., Hor, L.-I., & Amaro, C. (2015). Host–pathogen interactions in *Vibrio vulnificus*: responses of monocytes and vascular endothelial cells to live bacteria. *Future Microbiology*, *10*(4), 471–487. https://doi.org/10.2217/fmb.14.136

Newman, J. D., Chopra, J., Shah, P., Shi, E., McFadden, M. E., Horness, R. E., Brown, L. C., & van Kessel, J. C. (2021). Amino acid divergence in the ligand-binding pocket of Vibrio LuxR/HapR proteins determines the efficacy of thiophenesulfonamide inhibitors. *Molecular Microbiology*, *116*(4), 1173–1188. https://doi.org/10.1111/mmi.14804

Newman, J. D., Russell, M. M., Fan, L., Wang, Y. X., Gonzalez-Gutierrez, G., & Van Kessel, J. C. (2021). The DNA binding domain of the Vibrio vulnificus SmcR transcription factor is flexible and binds diverse DNA sequences. *Nucleic Acids Research*, *49*(10), 5967–5984. https://doi.org/10.1093/nar/gkab387

Newman, J. D., & van Kessel, J. C. (2021). Purification of the Vibrio Quorum-Sensing Transcription Factors LuxR, HapR, and SmcR. In *Methods in Molecular Biology* (Vol. 2346, pp. 173–182). Humana Press Inc. https://doi.org/10.1007/7651_2020_306

Newton, A., Kendall, M., Vugia, D. J., Henao, O. L., & Mahon, B. E. (2012). Increasing rates of vibriosis in the United States, 1996-2010: Review of surveillance data from 2 systems. In *Clinical Infectious Diseases* (Vol. 54, Issue SUPPL.5). https://doi.org/10.1093/cid/cis243

Paranjpye, R. N., & Strom, M. S. (2005). Colonization of shellfish by pathogenic Vibrios. *Proceedings of MTS/IEEE OCEANS, 2005*, *2005*, 1099–1103. https://doi.org/10.1109/OCEANS.2005.1639903

Piiadov, V., Ares de Araújo, E., Oliveira Neto, M., Craievich, A. F., & Polikarpov, I. (2019). SAXSMoW 2.0: Online calculator of the molecular weight of proteins in dilute solution from experimental SAXS data measured on a relative scale. *Protein Science*, *28*(2), 454–463. https://doi.org/10.1002/pro.3528

Pollock, F. J., Krediet, C. J., Garren, M., Stocker, R., Winn, K., Wilson, B., Huete-Stauffer, C., Willis, B. L., & Bourne, D. G. (2015). Visualization of coral host–pathogen interactions using a stable GFP-labeled Vibrio coralliilyticus strain. *Coral Reefs*, *34*(2), 655–662. https://doi.org/10.1007/s00338-015-1273-3

Rajamanikandan, S., Jeyakanthan, J., & Srinivasan, P. (2017a). Binding mode exploration of LuxR-thiazolidinedione analogues, e-pharmacophore-based virtual screening in the designing of LuxR inhibitors and its biological evaluation. *Journal of Biomolecular Structure and Dynamics*, *35*(4), 897–916. https://doi.org/10.1080/07391102.2016.1166455

Rajamanikandan, S., Jeyakanthan, J., & Srinivasan, P. (2017b). Discovery of potent inhibitors targeting Vibrio harveyi LuxR through shape and e-pharmacophore based virtual screening and its biological evaluation. *Microbial Pathogenesis*, *103*, 40–56. https://doi.org/10.1016/j.micpath.2016.12.003

Rémy, B., Mion, S., Plener, L., Elias, M., Chabrière, E., & Daudé, D. (2018). Interference in bacterial quorum sensing: A biopharmaceutical perspective. In *Frontiers in Pharmacology* (Vol. 9, Issue MAR). Frontiers Media S.A. https://doi.org/10.3389/fphar.2018.00203

875 Rutherford, S. T., Van Kessel, J. C., Shao, Y., & Bassler, B. L. (2011). AphA and LuxR/HapR reciprocally
876 control quorum sensing in vibrios. *Genes and Development*, *25*(4), 397–408.
877 https://doi.org/10.1101/gad.2015011

878 Schneidman-Duhovny, D., Hammel, M., Tainer, J. A., & Sali, A. (2013). Accurate SAXS Profile
879 Computation and its Assessment by Contrast Variation Experiments. *Biophysical Journal*, *105*(4),
880 962–974. https://doi.org/10.1016/j.bpj.2013.07.020

881 Schneidman-Duhovny, D., Hammel, M., Tainer, J. A., & Sali, A. (2016). FoXS, FoXSDock and MultiFoXS:
882 Single-state and multi-state structural modeling of proteins and their complexes based on SAXS
883 profiles. *Nucleic Acids Research*, *44*(W1), W424–W429. https://doi.org/10.1093/nar/gkw389

884 Sen, H., Choudhury, G. B., Pawar, G., Sharma, Y., Bhalerao, S. E., Chaudhari, V. D., Datta, S., &
885 Raychaudhuri, S. (2023). Diversity in the ligand binding pocket of HapR attributes to its uniqueness
886 towards several inhibitors with respect to other homologues - A structural and molecular
887 perspective. *International Journal of Biological Macromolecules*, *233*, 123495.
888 https://doi.org/10.1016/j.ijbiomac.2023.123495

889 Silva, A. J., & Benitez, J. A. (2016). Vibrio cholerae Biofilms and Cholera Pathogenesis. *PLOS Neglected*
890 *Tropical Diseases*, *10*(2), e0004330. https://doi.org/10.1371/journal.pntd.0004330

891 Singleton, F. L., Attwell, R. W., Jangi, M. S., & Colwell, R. R. (1983). Influence of Salinity, Nutrient
892 Concentration and Temperature on Growth and Survival of Vibrio Choleras in the Aquatic
893 Environment. In S. Kuwahara & N. F. Pierce (Eds.), *Advances in Research on Cholera and Related*
894 *Diarrheas* (pp. 101–112). Springer Netherlands. https://doi.org/10.1007/978-94-009-6735-9_12

895 Soto-Rodriguez, S. A., Gomez-Gil, B., Lozano-Olvera, R., Betancourt-Lozano, M., & Morales-Covarrubias,
896 M. S. (2015). Field and experimental evidence of Vibrio parahaemolyticus as the causative agent of
897 acute hepatopancreatic necrosis disease of cultured shrimp (Litopenaeus vannamei) in
898 northwestern Mexico. *Applied and Environmental Microbiology*, *81*(5), 1689–1699.
899 https://doi.org/10.1128/AEM.03610-14

900 Starkey, M., Lepine, F., Maura, D., Bandyopadhaya, A., Lesic, B., He, J., Kitao, T., Righi, V., Milot, S., Tzika,
901 A., & Rahme, L. (2014). Identification of Anti-virulence Compounds That Disrupt Quorum-Sensing
902 Regulated Acute and Persistent Pathogenicity. *PLoS Pathogens*, *10*(8).
903 https://doi.org/10.1371/journal.ppat.1004321

904 Swartzman, E., Silverman, M., & Meighen, E. A. (1992). The luxR gene product of Vibrio harveyi is a
905 transcriptional activator of the lux promoter. *Journal of Bacteriology*, *174*(22), 7490–7493.
906 https://doi.org/10.1128/jb.174.22.7490-7493.1992

907 Thompson, J. R., Randa, M. A., Marcelino, L. A., Tomita-Mitchell, A., Lim, E., & Polz, M. F. (2004).
908 Diversity and dynamics of a North Atlantic coastal Vibrio community. *Applied and Environmental*
909 *Microbiology*, *70*(7), 4103–4110. https://doi.org/10.1128/AEM.70.7.4103-4110.2004

910 Tu, K. C., & Bassler, B. L. (2007). Multiple small RNAs act additively to integrate sensory information and
911 control quorum sensing in *Vibrio harveyi*. *Genes & Development*, *21*(2), 221–233.
912 https://doi.org/10.1101/gad.1502407

913 Van Kessel, J. C., Rutherford, S. T., Shao, Y., Utria, A. F., & Bassler, B. L. (2013). Individual and combined
914 roles of the master regulators apha and luxr in control of the Vibrio harveyi quorum-sensing
915 regulon. *Journal of Bacteriology*, *195*(3), 436–443. https://doi.org/10.1128/JB.01998-12

916 van Kessel, J. C., Ulrich, L. E., Zhulin, I. B., & Bassler, B. L. (2013). Analysis of activator and repressor
917 functions reveals the requirements for transcriptional control by LuxR, the master regulator of
918 quorum sensing in Vibrio harveyi. *MBio*, *4*(4). https://doi.org/10.1128/mBio.00378-13

919 Verma, J., Bag, S., Saha, B., Kumar, P., Ghosh, T. S., Dayal, M., Senapati, T., Mehra, S., Dey, P.,
920 Desigamani, A., Kumar, D., Rana, P., Kumar, B., Maiti, T. K., Sharma, N. C., Bhadra, R. K., Mutreja,
921 A., Nair, G. B., Ramamurthy, T., & Das, B. (2019). Genomic plasticity associated with antimicrobial
922 resistance in *Vibrio cholerae*. *Proceedings of the National Academy of Sciences*, *116*(13), 6226–
923 6231. https://doi.org/10.1073/pnas.1900141116

924 Vezzulli, L., Grande, C., Reid, P. C., Hélaouët, P., Edwards, M., Höfle, M. G., Brettar, I., Colwell, R. R., &
925 Pruzzo, C. (2016). Climate influence on Vibrio and associated human diseases during the past half-
926 century in the coastal North Atlantic. *Proceedings of the National Academy of Sciences of the*
927 *United States of America*, *113*(34), E5062–E5071. https://doi.org/10.1073/pnas.1609157113

928 Visick, K. L. (2009). An intricate network of regulators controls biofilm formation and colonization by
929 *Vibrio fischeri*. *Molecular Microbiology*, *74*(4), 782–789. https://doi.org/10.1111/j.1365-
930 2958.2009.06899.x

931 Waters, C. M., & Bassler, B. L. (2005). QUORUM SENSING: Cell-to-Cell Communication in Bacteria.
932 *Annual Review of Cell and Developmental Biology*, *21*(1), 319–346.
933 https://doi.org/10.1146/annurev.cellbio.21.012704.131001

934 Wei, Y., Ocampo, P., & Levin, B. R. (2010). An experimental study of the population and evolutionary
935 dynamics of *Vibrio cholerae* O1 and the bacteriophage JSF4. *Proceedings of the Royal Society B:*
936 *Biological Sciences*, *277*(1698), 3247–3254. https://doi.org/10.1098/rspb.2010.0651

937 Werten, S., Waack, P., Palm, G. J., Virolle, M., & Hinrichs, W. (2023). Crystal structures of free and
938 ligand-bound forms of the <scp>TetR</scp> / <scp>AcrR-like</scp> regulator <scp>SCO3201</scp>
939 from *Streptomyces coelicolor* suggest a novel allosteric mechanism. *The FEBS Journal*, *290*(2), 521–
940 532. https://doi.org/10.1111/febs.16606

941 Yang, J. H., Mok, J. S., Jung, Y. J., Lee, K. J., Kwon, J. Y., Park, K., Moon, S. Y., Kwon, S. J., Ryu, A. R., & Lee,
942 T. S. (2017). Distribution and antimicrobial susceptibility of Vibrio species associated with
943 zooplankton in coastal area of Korea. *Marine Pollution Bulletin*, *125*(1–2), 39–44.
944 https://doi.org/10.1016/j.marpolbul.2017.07.054

945 Zamora-Pantoja, D. R., Quiñones-Ramírez, E. I., Fernández, F. J., & Vázquez-Salinas, C. (2013). Virulence
946 factors involved in the pathogenesis of Vibrio parahaemolyticus. *Reviews in Medical Microbiology*,
947 *24*(2), 41–47. https://doi.org/10.1097/MRM.0b013e32835a1f02

948 Zhang, J., Liu, B., Gu, D., Hao, Y., Chen, M., Ma, Y., Zhou, X., Reverter, D., Zhang, Y., & Wang, Q. (2021).
949 Binding site profiles and N-terminal minor groove interactions of the master quorum-sensing
950 regulator LuxR enable flexible control of gene activation and repression. *Nucleic Acids Research*,
951 *49*(6), 3274–3293. https://doi.org/10.1093/nar/gkab150

Figure 1

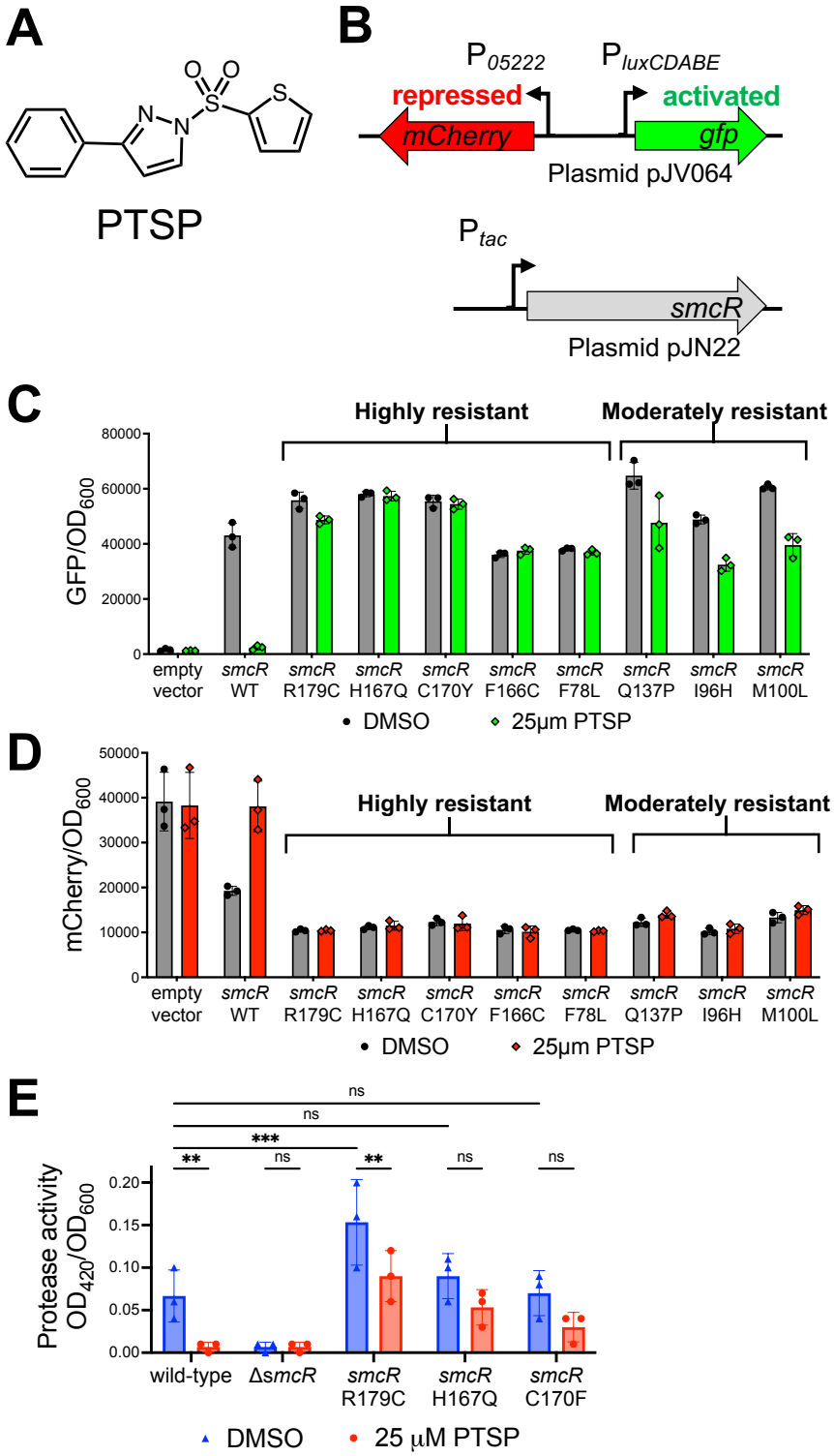

Figure 1. Forward genetic screen identifies mutant *smcR* alleles resistant to PTSP. (A) Structure of PTSP compound. (B) Diagram of the two-plasmid screen in *E. coli* in which wild-type or mutant *smcR* alleles encoded on plasmid pJN22 were screened for activity using a two-color reporter plasmid pJV064. The *luxCDABE* promoter is activated by SmcR and the *05222* promoter is repressed by SmcR. (C, D) *E. coli* strains contained plasmids pJN22 (wild-type *smcR* allele) or mutant pJN22 plasmids from library screening and pJV064. SmcR expression was induced with 50 µM IPTG and cultures treated with either 25 µM PTSP or an equal volume of DMSO solvent. GFP (C) and mCherry (D) relative to the OD_{600} were measured and plotted. (E) Protease activity (OD_{420}/OD_{600}) of wild-type and mutant *V. vulnificus* strains. Statistical analyses: a two-way analysis of variance (ANOVA) was performed on normally distributed data (Shapiro-Wilk test; n=3; **, p=0.01; ***, p=0.001).

Figure 2

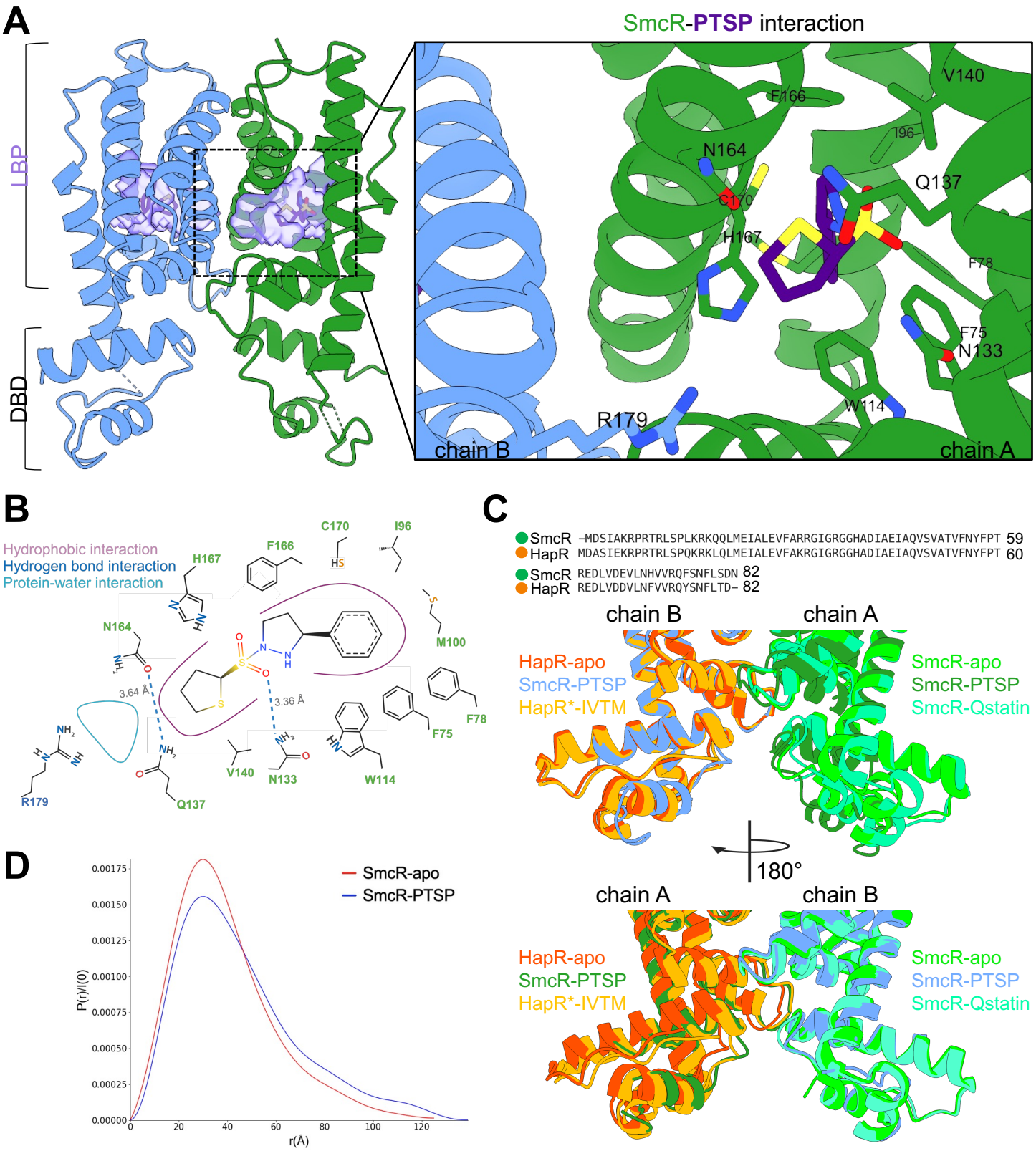

Figure 2. Structural basis for SmcR ligand binding. (A) X-ray crystal structure of homodimeric SmcR (blue/green) bound to PTSP (purple). Solvent accessible ligand binding pocket is shown as a surface in light purple (left). Residues important for contacting PTSP in the SmcR LBP (right). (B) 2D projection of the SmcR-PTSP binding interface showing hydrophobic contacts (purple lines), hydrogen bond interactions (blue), and solvent interactions (cyan). (C) Sequence and structural alignment of HapR and SmcR. The X-ray crystals structures of SmcR-apo (light green; PDB: 6WAE), SmcR-PTSP (colored by chain as in (A)) , SmcR-Qstatin (blue-green; PDB: 5X3R), HapR-apo (orange; 7XXO), and HapR*-ITVM (light orange; PDB: 7XYI). HapR* indicates the HapR quadruple variant from Sen et al. 2023 that stably binds to thiophenesulfonamide inhibitors. (D) The estimated pair-distance distribution function, P(r) normalized by the scattering intensity, I(0). The P(r) function is based on the Indirect Fourier Transform of SAXS data for SmcR-apo (red) and SmcR-PTSP (blue).

Figure 3

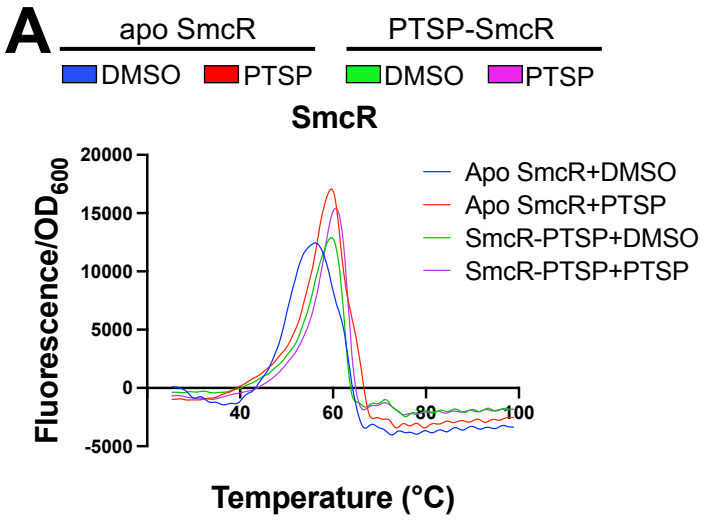

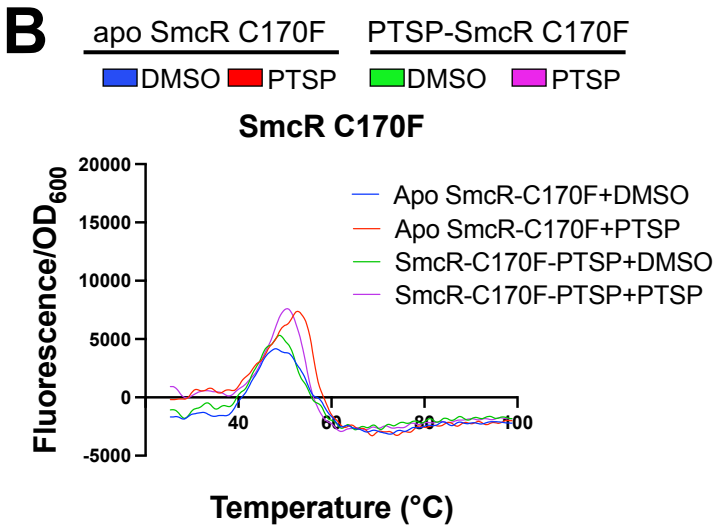

Figure 3. SmcR stability increases in the presence of PTSP. (A, B) Representative plots of thermostability data for wild-type SmcR (A) and SmcR C170F (B) proteins purified without PTSP (apo) or with PTSP. Either PTSP or an equivalent volume of DMSO were added to each reaction as indicated. Data are representative of three biological replicates.

Figure 4

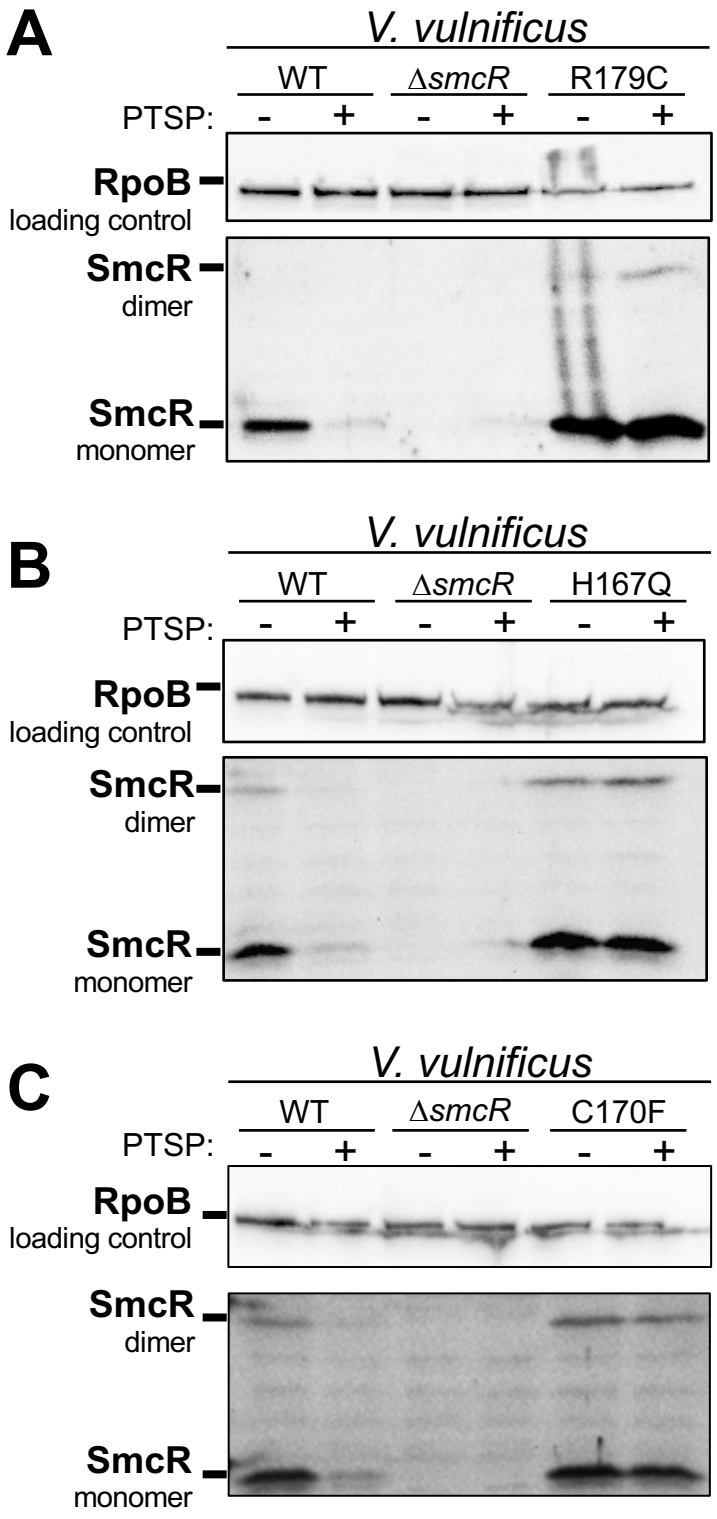

Figure 4. PTSP increases proteolytic degradation of SmcR *in vivo.* (A, B, C) Western blot analysis of SmcR protein levels in cell lysates from *V. vulnificus* strains wild-type, Δ*smcR*, and *smcR* R179C (A), H167Q (B), or C170F (C) with 25 μM 10B (+) or an equivalent concentration of DMSO solvent (-). Anti-RpoB antibodies were used as a loading control. Each panel is a representative of triplicate biological assays.

Figure 5

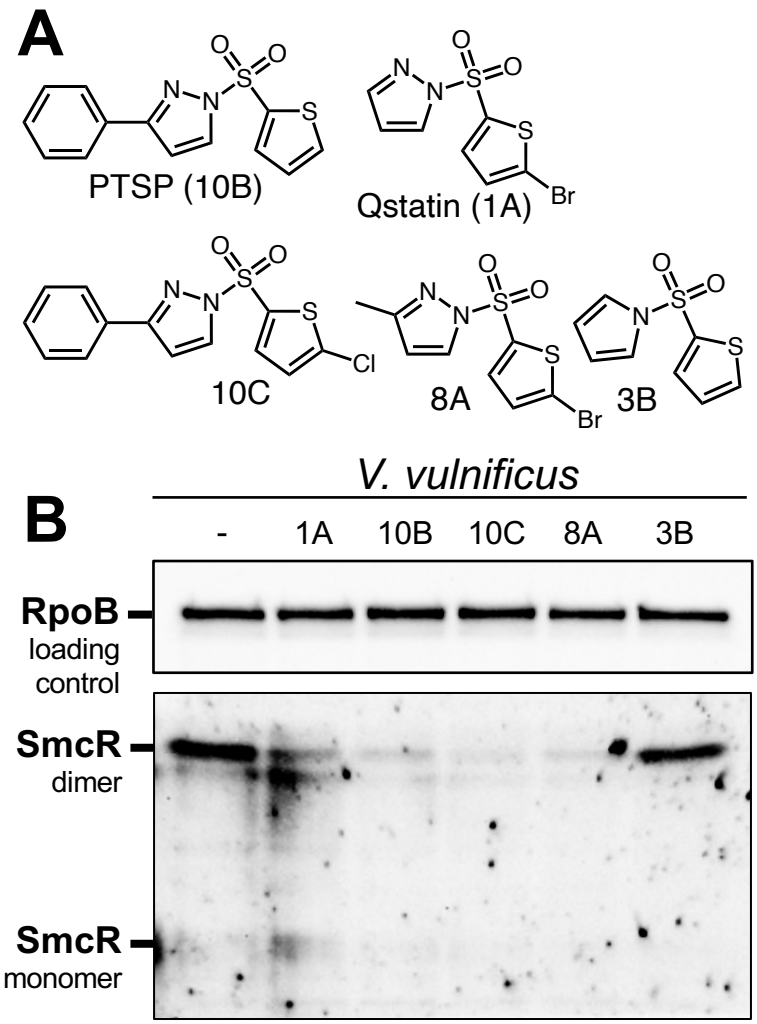

Figure 5. Thiophenesulfonamides cause proteolytic degradation of LuxR/HapR proteins in *Vibrio* species. (A) Structures of compounds used in assay shown in panel B. (B) Western blot analysis of cell lysates with anti-LuxR antibodies measuring SmcR from *V. vulnificus.* Cells were treated with 25 μM of each thiophenesulfonamide indicated or an equivalent concentration of DMSO solvent (-). Anti-RpoB antibodies were used as a loading control. Each panel is a representative of triplicate biological assays.

Figure 6

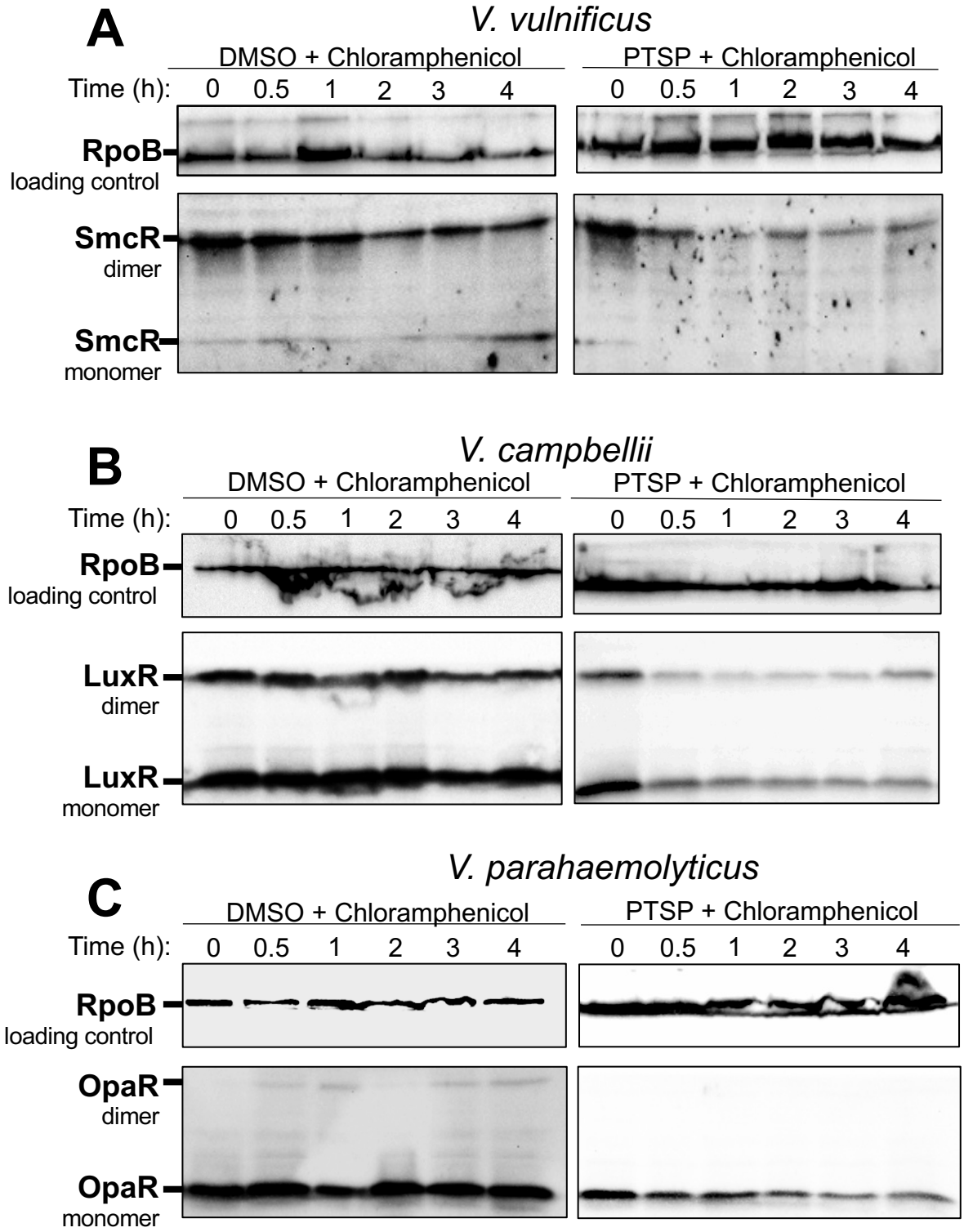

Figure 6. *In vivo* proteolytic cleavage of LuxR/HapR proteins in *Vibrio* species. (A, B, C) Western blot analysis of cell lysates with anti-LuxR antibodies measuring SmcR from *V. vulnificus* (A), LuxR from *V. campbellii* (B), or OpaR from *V. parahaemolyticus* (C) wild-type strains. Cells were either treated with 25 μM PTSP or an equivalent concentration of DMSO solvent and grown to an OD of 0.5-0.8. Translation was halted by addition of 10ug/ml of Chloramphenicol and pellets were harvested at 0, 30, 60, 120, 180 and 240 mins after that. Anti-RpoB antibodies were used as a loading control. Each panel is a representative of triplicate biological assays.

Figure 7

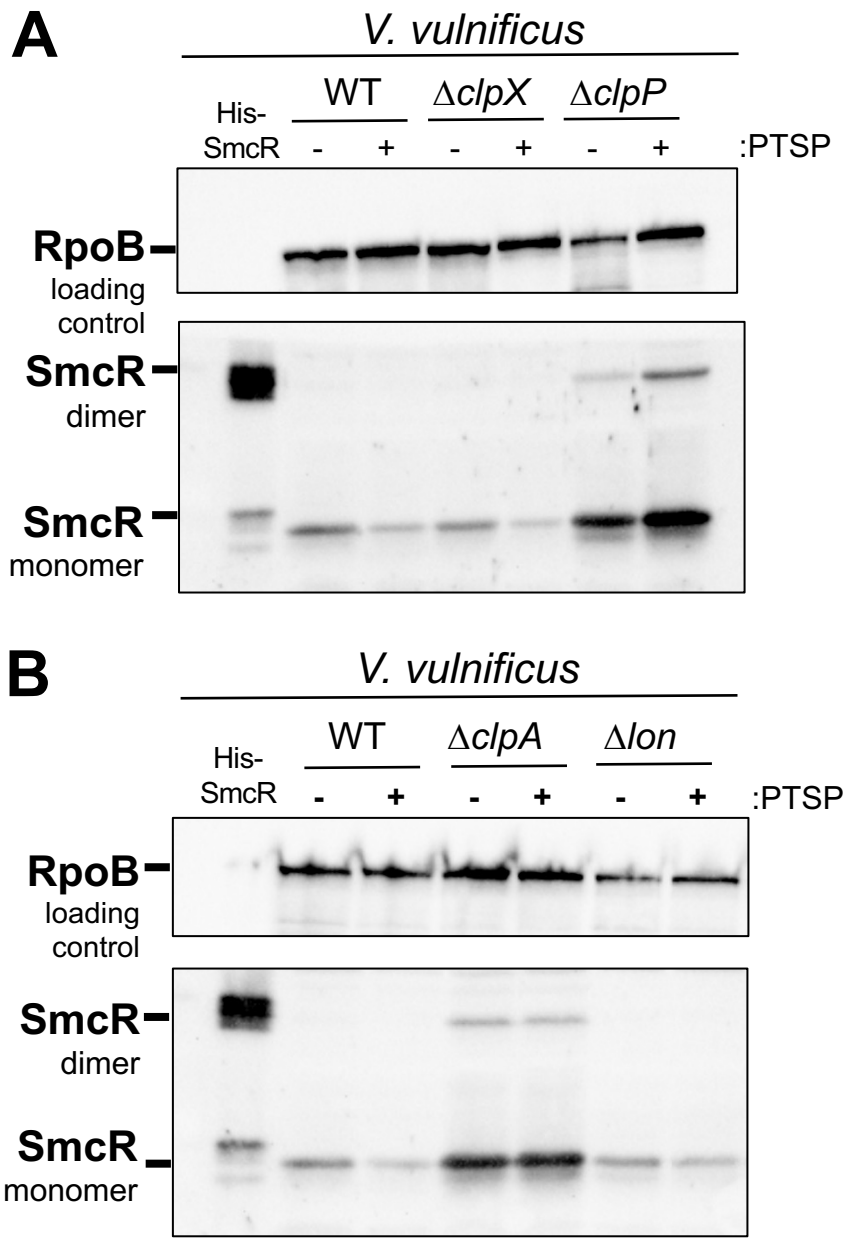

Figure 7. ClpAP proteolysis of SmcR is blocked by substitutions that block inhibitor binding. Western blot analysis of cell lysates measuring SmcR from *V. vulnificus* strains wild-type, Δ*clpX*, Δ*clpP*, Δ*clpA*, or Δ*lon*. Cells were treated with 25 μM of 10B or an equivalent concentration of DMSO solvent (-). Anti-RpoB antibodies were used as a loading control. Each panel is a representative of triplicate biological assays.

Figure 8

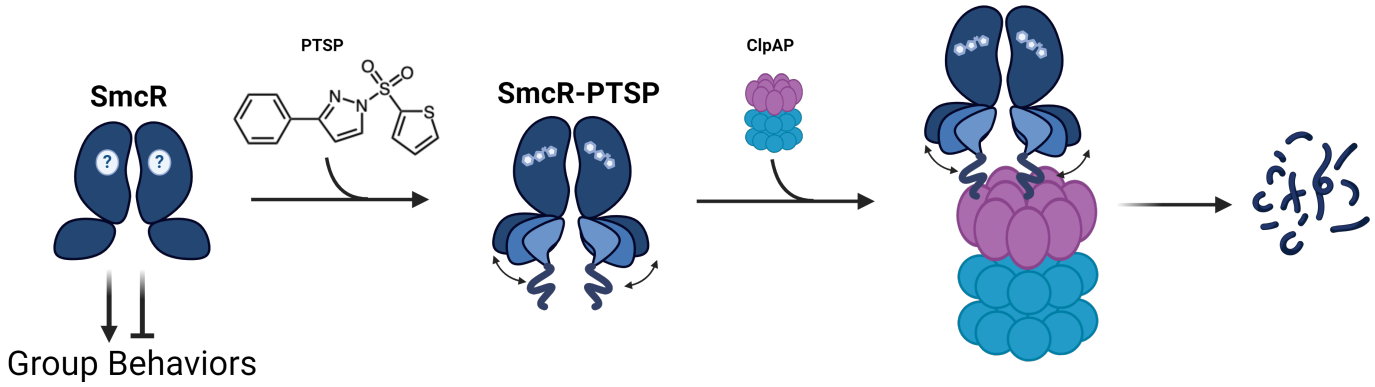

Figure 7. Model of SmcR degradation by ClpAP protease. SmcR bound to its native ligand (?, unknown) is active at high cell density and regulates genes encoding proteins that drive group behaviors (protease production, biofilm formation, toxin production, *etc.*). Addition of PTSP to cultures displaces the native ligand, driving an allosteric conformational change in the DNA binding domains of each SmcR monomer. The unfolded N-terminus is recognized by ClpAP and degraded.